Bulletin of the Seismological Society of America, Vol. 101, No. 2, pp. 596–618, April 2011, doi: 10.1785/0120090387

Ⓔ

Estimating Time Scales and Length Scales in Pulselike Earthquake Acceleration Records with Wavelet Analysis

by Michalis F. Vassiliou and Nicos Makris

Abstract This paper is motivated from the need to extract the characteristic time and length scales of strong pulselike ground motions with a mathematically formal, objective, and easily reproducible procedure. The investigation uses wavelet analysis to identify and extract energetic acceleration pulses (not velocity pulses) together with their associated frequency and amplitude. The processing of acceleration records with wavelet analysis is capable of extracting pulses that are not detected visually in the acceleration records, yet they become coherent and distinguishable in the velocity records. Most importantly, the proposed analysis is capable of extracting shorter duration distinguishable pulses (not necessarily of random character) that override the longer near-source pulses that are of significant engineering interest. The study elaborates on the role of the weighting function in the definition of the wavelet transform and concludes that longer pulses are captured when less suppressive weighting functions are implemented in the wavelet transform. We examine the capability of several popular symmetric and antisymmetric wavelets to locally match the energetic acceleration pulse. We conclude that the exercise to identify the best-matching wavelet shall incorporate, in addition to the standard translation and dilation-contraction of the wavelet transform, a phase modulation together with a manipulation of the oscillatory character (addition of cycles) of the wavelet. This need leads to the extension of the wavelet transform to a more general wavelet transform during which the mother wavelet is subjected to the four above-mentioned modulations. The mathematical definition and effectiveness of this extended wavelet transform is presented in this paper. The objective identification of the pulse period, amplitude, phase, and oscillatory character of pulselike ground motions with the extended wavelet transform introduced in this paper makes possible the immediate use of closed-form expressions published by other investigators to estimate the peak response of elastic and inelastic systems.

Online Material: Parameters that maximize the extended wavelet transform of 183 selected records.

Introduction

Ground motions that contain distinguishable, long-duration acceleration pulses impose severe deformation demands on structures, which occasionally exhaust the deformation capacity of structural members or even the entire structural system. Following the spectacular damage of the Olive View Hospital during the 1971 San Fernando, California, earthquake, Bertero *et al.* (1978) directed the attention of engineers to long-duration acceleration pulses (1–1.5 s long at that time), which result in unusually large monotonic velocity increments. During the subsequent 15 yr, there have been a handful of publications that stressed the significance of long-duration pulses (Bertero *et al.*, 1991; Somerville and Graves, 1993); however, it was only after the 1994 Northridge, California, and the 1995 Kobe, Japan, earthquakes that the majority of engineers recognized the severe implications and the destructive potential of pulselike ground motions recorded near the causative fault of earthquakes (Hall *et al.*, 1995). The destructive potential of pulselike ground motions was further confirmed after the 1999 Izmit, Turkey, and the 1999 Chi-Chi, Taiwan, earthquakes (Ma *et al.*, 2001; Loh *et al.*, 2000; Wang *et al.*, 2001; Sekiguchi and Iwata, 2002).

In some near-source events, the pulse is also distinguishable in the acceleration history, and in this case, the ground motions are particularly destructive to most civil structures. In other cases, acceleration records contain high-frequency spikes and resemble random motions; however, their velocity

and displacement histories uncover a coherent long-duration pulse that results from the nonzero mean of the acceleration fluctuations. These motions have a much smaller destructive potential for most civil structures ($T_s < 4$ s) even when they produce ground displacements as large as 3 m. A comprehensive comparison between the destructive potential of these two classes of near-source ground motions was presented by Makris and Black (2004c). The area under the acceleration pulse was coined by Bertero as the incremental ground velocity in an effort to distinguish between the net increment of the ground velocity along a monotonic segment of its time history and the peak ground velocity that might be the result of the summation of a succession of high-frequency, one-sided acceleration spikes. It seems that the subtle distinction made by Bertero *et al.* (1978) did not receive the attention it deserves because, in several occasions, a long velocity pulse and its peak value are invariably used to express the damaging potential of ground motions (Spence *et al.*, 1992; Naeim, 1995, among others). Accordingly, this paper focuses on matching and extracting coherent acceleration pulses (not velocity pulses) of strong ground motions.

Mathematical Representation of Coherent Pulses

The relatively simple form, yet destructive potential of the prevailing coherent pulse of near-source ground motions has motivated the development of various closed-form expressions that approximate their leading kinematic characteristics. The early work of Veletsos *et al.* (1965) was followed by the papers of Hall *et al.* (1995), Makris (1997), Makris and Chang (2000), Alavi and Krawinkler (2001), Menum and Fu (2002), Mavroeidis and Papageorgiou (2003), and Mavroeidis *et al.* (2004), among others. Some of the proposed pulses are physically realizable motions with zero final ground velocity and finite accelerations, whereas other idealizations violate one or both of the above requirements. Physical realizable pulses can satisfactorily describe the impulsive character of near-fault ground motions, both qualitatively and quantitatively. The minimum number of parameters is two; these are either the pulse duration, T_p, and acceleration amplitude, a_p, or the pulse duration, T_p, and velocity amplitude, v_p (Makris, 1997; Makris and Chang, 2000). The more sophisticated model of Mavroeidis and Papageorgiou (2003) that was motivated from the Gabor (1946) elementary signals involves 4 parameters: the pulse period, T_p, the pulse amplitude, A, as well as the phase angle, φ, and the oscillatory character, γ, of the signal.

In the Mavroeidis and Papageorgiou (2003) paper, the parameters T_p, A, φ, and γ are not estimated by any formal procedure, but by a step-by-step procedure which involves judgment of the user. For instance, the pulse period, T_p, is determined so that the pseudo-velocity response spectra of the synthetic and recorded near-fault ground motions exhibit their peak values at approximately the same natural period. Parameter A is determined so that the amplitude of the synthetic velocity pulse and its peak pseudospectral velocity agree well with the corresponding quantities of the actual record, while parameters φ and γ are adjusted so as to fit by trial and error the synthetic velocity and displacement records and by readjusting parameter A.

A challenge, however, that often appears in several near-source records is that, in addition to the coherent pulse associated with the near-source effect, there is a shorter duration distinguishable pulse (not necessarily of random character) that overrides the longer duration near-source pulse. In several occasions, these shorter duration pulses, which generate a second peak in the pseudovelocity spectrum, have significant engineering interest to a wide family of structures, and there is a need to identify and characterize them. For instance, Figure 1 portrays the north–south component of the acceleration, velocity, and displacement histories recorded at the TCU052 station during the 21 September 1999 Chi-Chi, Taiwan, earthquake. This record contains a 10-s long velocity pulse (the one associated with near-source effects), which is disturbed by a shorter, distinguishable pulse of duration about 2.0 s. This shorter, overriding pulse is of major engineering interest because it is responsible for most of the base shear and peak deformations of elastic and inelastic structures that are of interest in civil engineering (Makris and Black, 2004c). The bottom plots in Figure 1 show with a thin line the pseudovelocity spectrum of the TCU052 north–south record, which exhibits two peaks, one at about 2.0 s (due to the shorter period overriding pulse) and the other at about 9.0 s (due to the long-period pulse associated with the near-source directivity effects). The heavy lines in Figure 1 are synthetic pulses that are constructed by employing the step-by-step method as outlined in the Mavroeidis and Papageorgiou (2003) paper. Note that the exercise in fitting the short period pulse becomes challenging due to the presence of the carrier long-period pulse (velocity and displacement are out of place). Given (1) the iterative nature and the involvement of user judgment in the step-by-step method proposed by Mavroeidis and Papageorgiou (2003), (2) the engineering interest of local, shorter duration acceleration pulses, and (3) that the maximum inelastic displacement of structures scales with T_p^2 (the square of the period of the energetic pulse, see next section), the need for a mathematically formal, objective, and easily reproducible procedure to extract pulse periods and pulse amplitudes from pulselike ground motions becomes apparent. This need is the main motivation for this work.

While the aforementioned studies focused on the mathematical representation of distinguishable acceleration and velocity pulses, the first systematic study for quantitatively identifying coherent velocity pulses in near-fault ground motions was presented by Baker (2007). Baker's work uses wavelet analysis to automatically extract the largest velocity pulse (not acceleration pulse) in a given earthquake record; therefore, it offers some characteristic time and length scales of the ground motion. The limitation of processing velocity records with wavelet analysis is that one can only extract the visible main velocity pulse, usually the one that is associated with near-source effects. Baker (2007)

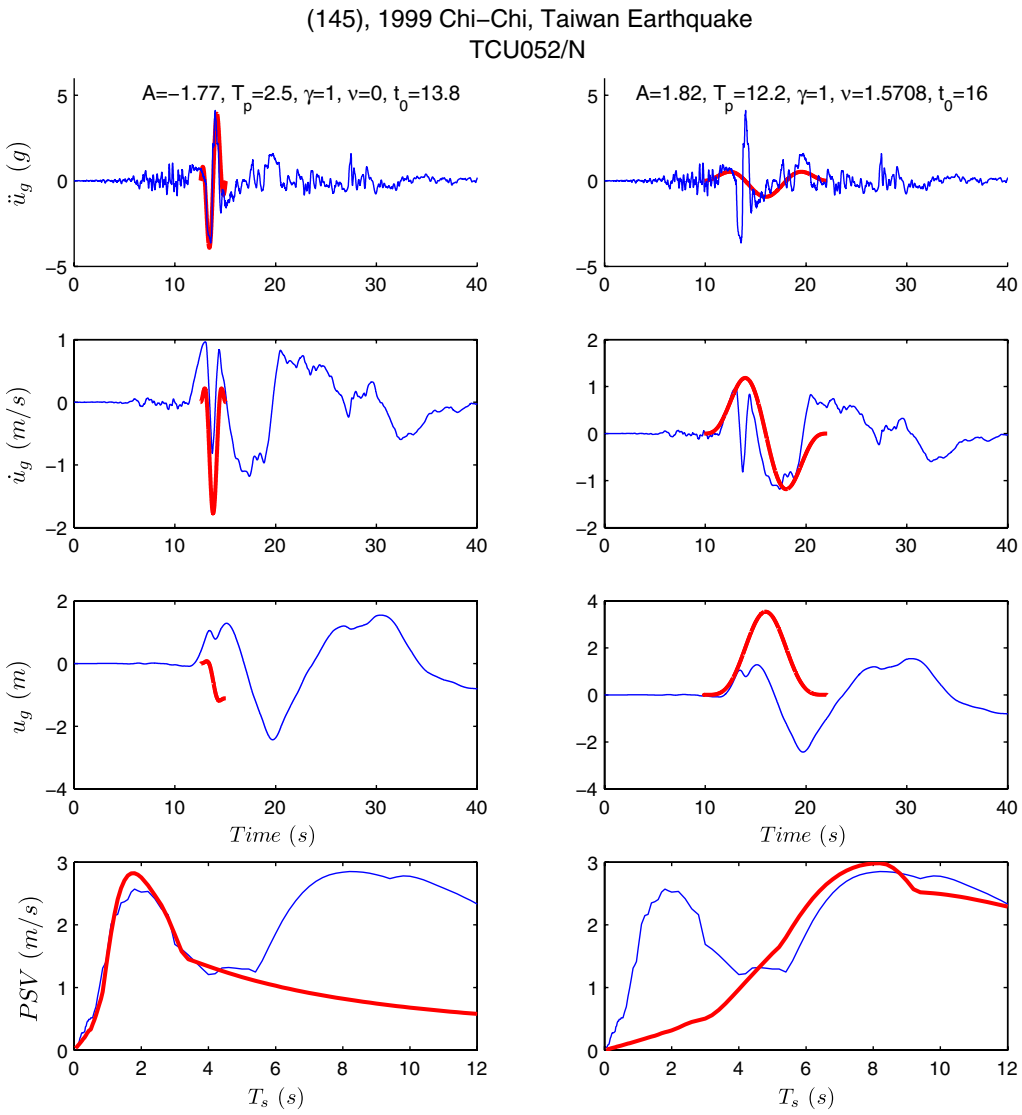

Figure 1. Top: Acceleration, velocity, and displacement time histories of the TCU052 north-south record from the 1999 Chi-Chi Taiwan earthquake. Heavy lines are the short-duration and long-duration pulses obtained with the step-by-step method offered in the Mavroeidis and Papageorgiou (2003) paper. Bottom: Pseudovelocity spectra. The color version of this figure is available only in the electronic edition.

recognized that in several occasions of his analysis (in which all daughter wavelets had the same energy—the default setting in the MATLAB Wavelet Toolbox [see Data and Resources section]), the pulse periods obtained from the wavelet analysis differ significantly from the pulse periods obtained from the velocity spectrum analysis (see fig. 12 of his paper), and he correctly explained that the pulse period extracted with the maximum spectral velocity is associated, in general, with a high-frequency oscillatory portion of the ground motion, whereas the pulse extracted with the wavelet analysis is associated with the main velocity pulse.

One of the advantages of this work, where we process acceleration records, is that the wavelet analysis can zoom into shorter duration distinguishable pulses (not necessarily of random character) that override the long-duration, near-source pulse. Such shorter duration pulses can outshine (in the scalogram, that is, the outcome of the wavelet transform) the main pulse associated with the near-source effect by selecting the appropriate weighting function in the wavelet transform (that does not necessarily preserve energy, the Euclidian norm of the wavelet, but rather it preserves some other norm of the wavelet). As an example, Figure 2 shows the best-matching wavelets on the acceleration time history of the TCU052 north–south motion recorded during the 1999 Chi-Chi, Taiwan, earthquake and the resulting velocity signals. The short (center) and long (right) period pulses shown emerged by selecting a weighting function in the wavelet transform that preserves in all daughter wavelets the same energy (center) and the same amplitude (right). Note that according to the selection of the weighting function, the proposed wavelet analysis on the acceleration record captures either the shorter duration ($T_p = 1.75$ s)

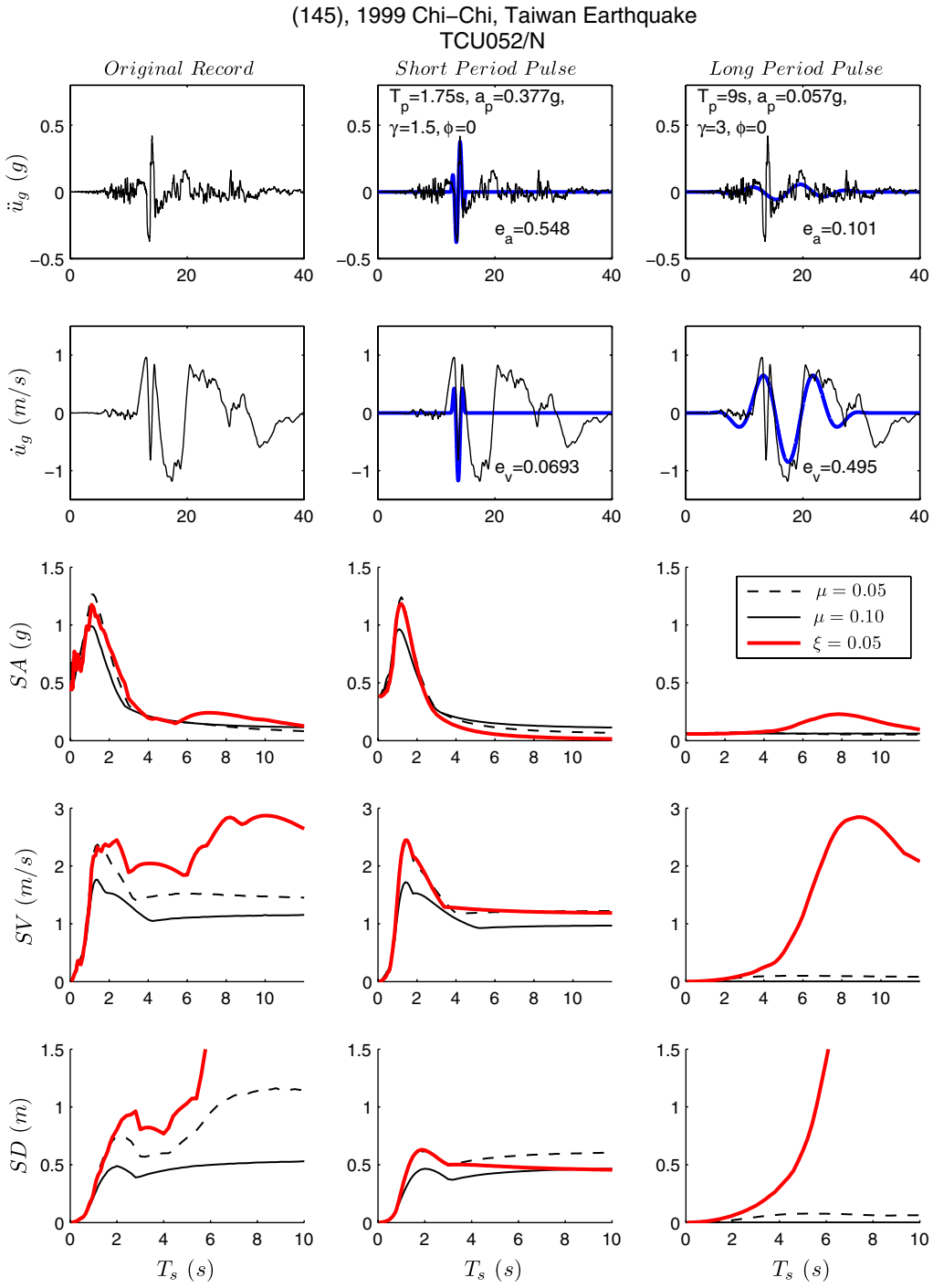

Figure 2. Total acceleration, relative velocity, and relative displacement spectra of a linear (m, k, c) and frictional (m, k, μ) oscillator subjected to the recorded motion (left), the short period pulse (center), and the long-period pulse that is associated with the near-source effects (right). The color version of this figure is available only in the electronic edition.

distinguishable pulse (center graphs) or the longer duration ($T_p = 9.0$ s) pulse associated with the near-source effects.

The availability of a mathematically formal numerical tool that automatically extracts the distinct time scales and length scales of ground motions, as first proposed by Baker (2007) and further developed in this work, is most attractive in earthquake engineering because it makes possible the use of dimensional analysis, which brings forward the physical similarities that prevail in nonlinear structural response (Makris and Black, 2004a,b; Makris and Psychogios, 2006; Karavassilis *et al.*, 2010). Physical similarity is a decisive symmetry that shapes nonlinear behavior and may directly relate structural response quantities to the physical parameters of the faulting and wave-propagation processes. This

article essentially builds upon the work of Baker (2007), Gabor (1946), Mavroeidis and Papageorgiou (2003), and Makris and Black (2004c) in an effort to extract in a mathematically rigorous and objective way the parameters of the Mavroeidis and Papageorgiou (2003) model which best describe the most energetic acceleration pulse. Once the parameters of the energetic pulse are established with the proposed method, one can use the closed-form approximate expressions offered by Mavroeidis *et al.* (2004) or Karavassilis *et al.* (2010) to estimate with confidence the peak response of elastic and inelastic systems to pulselike ground motions.

In this work, we first examine with continuous wavelet transform 183 acceleration records using five elementary mother wavelets, and we conclude that not only the period (dilation-contraction of the wavelet) but also the phase and number of cycles (oscillatory character) need to be manipulated in order to achieve the best local matching of the prevailing acceleration pulse. Accordingly, the acceleration records of strong ground motions are represented mathematically by the time derivative of the Gabor (1946) elementary signal (or its variation proposed by Mavroeidis and Papageorgiou (2003)), and the concept of the wavelet transform is extended so that the mother wavelet is not only translated and dilated but also subjected to an appropriate phase shift and enhanced with additional cycles.

Length Scale of Ground Excitations That is Relevant to Structural Response

Within the context of earthquake engineering, an early solution to the response of a rigid-plastic system (rigid mass sliding on a moving base) subjected to a rectangular acceleration pulse was presented by Newmark (1965). Figure 3 (top left) shows a rigid mass, m, supported by a moving surface with coefficient of friction μ. Under a rectangular acceleration pulse with amplitude a_p and duration T_p, the maximum relative displacement of the mass on the moving surface is (Newmark, 1965)

$$u_{\max} = \frac{a_p T_p^2}{2}\left(\frac{a_p}{\mu g} - 1\right), \qquad (a_p > \mu g). \tag{1}$$

Equation (1) indicates that the maximum sliding (inelastic) displacement is proportional to the square of the duration of the pulse (pulse period), T_p^2, while it depends also on the intensity of the acceleration pulse, a_p. The product $a_p T_p^2 = L_p$ is a characteristic length scale (in this case, two times the displacement of the base when the acceleration pulse expires) of the ground excitation and is a measure of the persistence of the excitation pulse to generate inelastic deformation (sliding). The term in the parenthesis in equation (1) expresses the intensity of the pulse. While the rectangular acceleration pulse used by Newmark (1965) is not physically realizable by earthquake shaking (infinite ground displacement), it is probably the most well-suited example to introduce the finite length scale, $L_p = a_p T_p^2$, of the energetic pulse of the motion that eventually leads to an infinite ground displacement. Upon the expiration of the pulse, the base moves with a constant velocity, and the inertia demand on the structure is zero.

In order that the ground assumes a zero velocity at the expiration of the pulse, the positive rectangular acceleration pulse used by Newmark needs to be followed by an equal-area negative acceleration pulse as shown in Figure 3 (right). This acceleration pulse is defined as

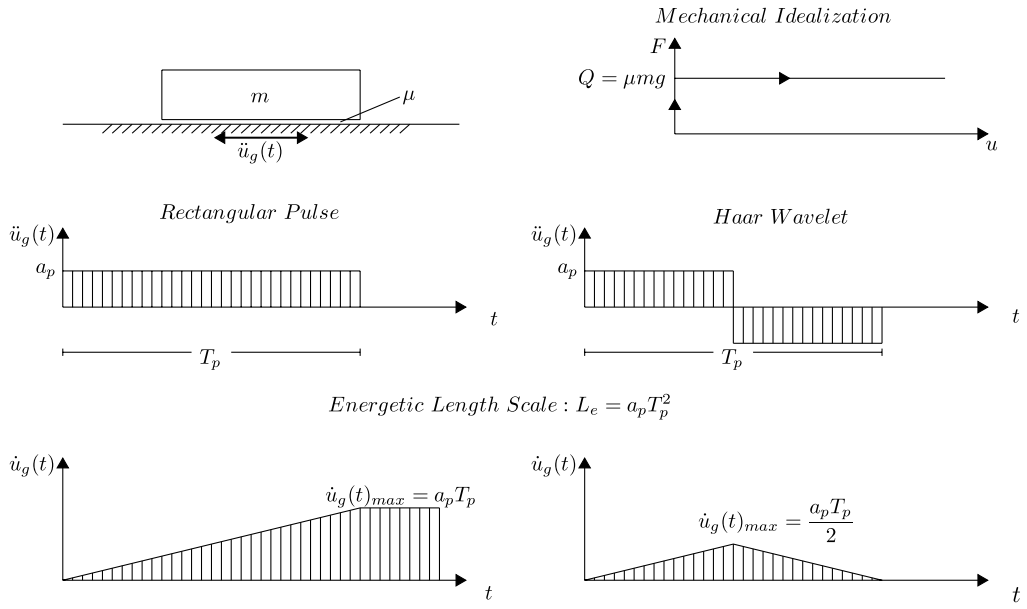

Figure 3. Top: Sliding mass resting on a horizontal plane and the mechanical idealization of sliding resistance. Center: Rectangular acceleration pulse and Haar wavelet. Bottom: Velocity time histories of the acceleration pulses shown above.

$$\ddot{u}_g(t) = \psi(t) = \begin{cases} a_p, & 0 \le t < \frac{T_p}{2} \\ -a_p, & \frac{T_p}{2} \le t \le T_p \\ 0 & \text{elsewere} \end{cases}, \qquad (2)$$

and is known in the literature as the Haar wavelet (Mallat, 1999; Addison, 2002; among others).

When the ground is subjected to the Haar wavelet given by equation (2), the maximum sliding displacement of the mass is computed via simple integration of the equation of motion

$$u_{\max} = \frac{a_p T_p^2}{4}\left(\frac{a_p - \mu g}{a_p + \mu g}\right)$$
$$\Rightarrow \frac{u_{\max}}{a_p T_p^2} = \frac{1}{4}\left(\frac{\frac{a_p}{\mu g} - 1}{\frac{a_p}{\mu g} + 1}\right), \qquad (a_p > \mu g). \qquad (3)$$

Equation (3) is of the same form as equation (1), in which the term $a_p T_p^2$ expresses the persistence of the pulse to generate sliding, while the term in the parentheses is a measure of its intensity. Equation (3) dictates that once the pulse is strong enough to generate sliding ($\frac{a_p}{\mu g} > 1$), the maximum sliding (inelastic) displacement is again proportional to the square of the period of the acceleration pulse, T_p^2.

The scaling of the maximum displacement of the sliding mass (purely inelastic system) with T_p^2 shown in equation (3) was obtained by solving the differential equation of motion. The same results can be obtained with dimensional analysis of the physical problem (Makris and Black, 2004a). In the interest of completeness we show with dimensional analysis that the peak response of the elastic and elastoplastic single-degree-of-freedom (SDOF) systems also scales with T_p^2.

Consider an SDOF elastic oscillator with mass m, stiffness, $k = m\omega_0^2 = m\frac{4\pi^2}{T_0^2}$, and damping constant, $c = 2\xi m\omega_0$, that is subjected to a given acceleration pulse with duration T_p and acceleration amplitude a_p. The maximum relative-to-the-ground displacement of the SDOF oscillator, $u_{\max}$, is a function of four variables:

$$u_{\max} = f(T_0, \xi, a_p, T_p). \qquad (4)$$

The five variables appearing in equation (4), $u_{\max} \doteq [L]$, $T_0 \doteq [T]$, $\xi \doteq [1]$, $a_p \doteq [L][T]^{-2}$, and $T_p \doteq [T]$, involve only two reference dimensions: that of length $[L]$ and time $[T]$. According to Buckingham's Π theorem (Langhaar, 1951; Housner and Hudson, 1959), the number of independent dimensionless products (Π terms) is equal to the number of variables appearing in the equation that describe the physical problem (five variables in equation 4) minus the number of reference dimensions (two reference dimensions in equation 4). Therefore, for the linear SDOF oscillator we have $5 - 2 = 3$ dimensionless Π terms: $\Pi_m = \frac{u_{\max}}{a_p T_p^2}$, $\Pi_\omega = \frac{T_0}{T_p}$, $\Pi_\xi = \xi$; and equation (4) condenses to an equation that involves two variables only:

$$\Pi_m = \frac{u_{\max}}{a_p T_p^2} = \varphi\left(\frac{T_0}{T_p}, \xi\right) \Rightarrow u_{\max} = a_p T_p^2 \varphi\left(\frac{T_0}{T_p}, \xi\right). \qquad (5)$$

In the case of an elastoplastic system with mass m, yield strength Q, and yield displacement u_y that is subjected to a given acceleration pulse with duration T_p and acceleration amplitude a_p, the maximum relative-to-the-ground displacement of the SDOF oscillator, $u_{\max}$ is a function of four variables:

$$u_{\max} = f\left(\frac{Q}{m}, u_y, a_p, T_p\right). \qquad (6)$$

Again the number of reference dimensions is two ($[L], [T]$); therefore, for the elastoplastic system, the number of dimensionless Π terms is $5 - 2 = 3$, and equation (6) condenses to an equation that involves two variables only:

$$\Pi_m = \frac{u_{\max}}{a_p T_p^2} = \varphi\left(\frac{Q}{m a_p}, \frac{u_y}{a_p T_p^2}\right)$$
$$\Rightarrow u_{\max} = a_p T_p^2 \varphi\left(\frac{Q}{m a_p}, \frac{u_y}{a_p T_p^2}\right). \qquad (7)$$

As in equation (3), equations (5) and (7) show that the maximum relative-to-the-ground displacement of the elastic and elastoplastic SDOF systems is also proportional to the square of the period of the acceleration pulse, T_p^2.

The similarities that exhibit the normalized inelastic response, $\Pi_m = u_{\max}\omega_p^2/a_p$, of three elastoplastic frames with strength, Q, and yield displacement, u_y, when excited by a set of 10 pulselike ground motions was examined in the paper by Makris and Psychogios 2006. Via regression analysis on the available data, that study concluded with the following expression for estimating the maximum inelastic displacement of frames with elastoplastic behavior:

$$u_{\max} = \frac{a_p}{\omega_p^2}\left(-0.46 + 2.4\frac{u_y\omega_p^2}{a_p}\right)\left(\frac{Q}{m a_p}\right)^{-0.57}. \qquad (8)$$

A more extended investigation that involved 216 multistory elastoplastic, steel, moment-resisting frames and 17 pulselike ground motions has recently been conducted by Karavassilis *et al.* (2010). In this latest study, equation (8) has been refined to

$$u_{\max} = \frac{a_p}{\omega_p^2}\left(-3.1 + 4.7\frac{u_y\omega_p^2}{a_p}\right)\left(\frac{Q}{m a_p}\right)^{-0.24}, \qquad (9)$$

given the wider set of data.

Certainly, the true inelastic displacement, $u_{\max}$, will depart from the estimation expression given by equations (8) or (9) (see, for example, fig. 11 of the Makris and Psychogios, 2006, paper or fig. 7 of the Karavassilis *et al.*, 2010, paper) for the very reason that the characteristic length scale

identified does not reflect the entire shaking potential of the recorded motion. On the other hand, however, the normalization of $u_{\max}$ with $a_p T_p^2$ (even when the acceleration pulse is diluted with overriding fluctuations) brings remarkable order in the inelastic response of structures, and the estimation expression given by equation (9) outperforms the prediction of other practical expressions (which hinge upon the elastic oscillator) to estimate inelastic deformation, such as those offered by Ruiz-Garcia and Miranda (2003) or Chopra and Chintanapakdee (2004).

Given that: (1) the ultimate scope of this effort is to investigate how the maximum elastic and inelastic displacement of engineering structures scales with the characteristic length scale of the energetic acceleration pulse, $L_p = a_p T_p^2$; and (2) the characteristic length scale is proportional to the square of the time scale of the excitation, T_p^2, this article investigates with wavelet analysis the coherent structure of 183 strong ground motions and develops a mathematically formal and easily reproducible procedure to extract the prevailing acceleration pulse period, T_p, and pulse amplitude, a_p, of their potential pulselike character.

Wavelet Analysis

Over the last two decades, wavelet transform analysis has emerged as a unique new time-frequency decomposition tool for signal processing and data analysis. There is a wide literature available regarding its mathematical foundation and its applications (Daubechies, 1992; Mallat, 1999; Addison, 2002, and references reported therein). Wavelets are simple wavelike functions localized on the time axis. For instance, the Haar wavelet shown in Figure 3 (center right) and expressed by equation (2), or the second derivative of the Gaussian distribution, $e^{-t^2/2}$, known in the seismology literature as the symmetric Ricker Wavelet (Ricker 1943, 1944) and widely referred as the Mexican Hat wavelet, (Addison, 2002),

$$\psi(t) = (1 - t^2)e^{-t^2/2}, \tag{10}$$

are widely used wavelets.

In order for a wavelike function to be classified as a wavelet, the wavelike function must have (1) finite energy,

$$E = \int_{-\infty}^{\infty} |\psi(t)|^2 dt < \infty; \tag{11}$$

and (2) a zero mean. In this work we are merely interested in achieving the best local matching of any given acceleration record with a wavelet that will offer the best estimates of the period (T_p = time scale) and amplitude (a_p, because $a_p T_p^2$ = length scale) of the prevailing energetic pulse. Accordingly, we perform a series of inner products (convolutions) of the ground acceleration signal, $\ddot{u}_g(t)$, with the wavelet ψ(t) by manipulating the wavelet through a process of translation (i.e., movement along the time axis) and a process of dilation-contraction (i.e., spreading out or squeezing of the wavelet):

$$C(s, \xi) = w(s) \int_{-\infty}^{\infty} \ddot{u}_g(t) \psi\left(\frac{t - \xi}{s}\right) dt. \tag{12}$$

The values of $s = S$ and $\xi = \Xi$ for which the coefficient, $C(s, \xi) = C(S, \Xi)$, reaches the maximum value offer the scale and location of the wavelet $w(s)\psi(\frac{t-\xi}{s})$ that locally best matches the acceleration record, $\ddot{u}_g(t)$. Equation (12) is the definition of the wavelet transform. The quantity $w(s)$ outside the integral in equation (12) is a weighting function. Typically, $w(s)$ is set equal to $1/\sqrt{s}$ in order to ensure that all wavelets $\psi_{s,\xi}(t) = w(s)\psi(\frac{t-\xi}{s})$ at every scale, s, have the same energy, and according to equation (11),

$$\int_{-\infty}^{\infty} |\psi_{s,\xi}(t)|^2 dt = \int_{-\infty}^{\infty} \left| \frac{1}{\sqrt{s}} \psi\left(\frac{t - \xi}{s}\right) \right|^2 dt = \|\psi_{s,\xi}(t)\|_2 = \text{constant}, \quad \forall\ s. \tag{13}$$

The same energy requirement among all the daughter wavelets $\psi_{s,\xi}(t)$ is the default setting in the 2007 MATLAB Wavelet Toolbox and what was used by Baker (2007); however, the same energy requirement is, by all means, not a restriction. Clearly, there are applications where it is more appropriate that all daughter wavelets, $\psi_{s,\xi}(t)$, at every scale, s, enclose the same area (not same energy) and, in this case, $w(s) = 1/s$; therefore,

$$\int_{-\infty}^{\infty} |\psi_{s,\xi}(t)| dt = \int_{-\infty}^{\infty} \left| \frac{1}{s} \psi\left(\frac{t - \xi}{s}\right) \right| dt = \|\psi_{s,\xi}(t)\|_1 = \text{constant}, \quad \forall\ s. \tag{14}$$

On the other hand, there may be applications where it is more appropriate that all daughter wavelets have merely the same maximum value and, in this case, $w(s) = 1$ and

$$\|\psi_{s,\xi}(t)\|_\infty = \text{constant}, \quad \forall\ s. \tag{15}$$

Figure 4 shows how a symmetric Ricker wavelet dilates when each of the three weighting functions are used.

A weighting function, $w(s) = 1/s^1 = 1/s$, suppresses the large-scale wavelets; therefore, it accentuates the presence of shorter period pulses, whereas a weighting function, $w(s) = 1/s^0 = 1$, accentuates the presence of longer period pulses. Figure 5 shows the acceleration, velocity, and displacement time histories recorded at the Pacoima Dam station during the 9 February 1971 San Fernando, California, earthquake with M_w 6.7. The heavy dashed line presents the wavelet $\lambda(S, \Xi)w(S)\psi(\frac{t-\Xi}{S})$, in which Ξ and S are the values of $s = S$ and $\xi = \Xi$ that give the maximum coefficient $C(S, \Xi)$ from equation (12), in which $w(s) = 1/\sqrt{s}$. The multiplication quantity

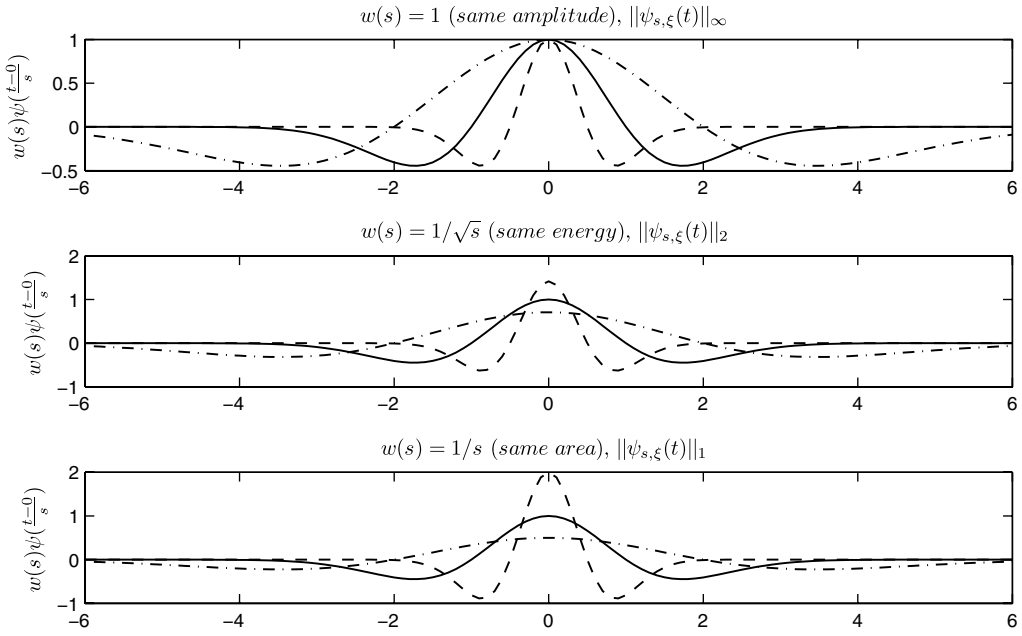

Figure 4. Comparison of symmetric Ricker wavelets when different weighting functions, $w(s)$, are used.

$$\lambda(S,\Xi) = \frac{C(S,\Xi)}{w^2(S)\cdot S\cdot E}, \tag{16}$$

which is derived in Appendix A, is needed in order for the best-matching wavelet, $\psi_{S,\Xi}(t) = w(s)\psi(\frac{t-\Xi}{S})$, to locally assume the amplitude of the acceleration record. In this case, the wavelet transform given by equation (12) captures the long-period pulse identified by Bertero *et al.* (1978) with $T_p = 1.35$ s. On the other hand, the heavy continuous line presents the wavelet $\psi(\frac{t-\Xi}{s})$, in which S and Ξ give the maximum coefficient, $C(S,\Xi)$, from equation (12), in which, now, $w(s) = 1/s$. The scalograms at the bottom of Figure 5 show the scale and the time instant when the wavelet transform $C(s,\xi)$ reaches its maximum for the two weighting functions examined. Accordingly, the selection of the weighting function has a dominant role in extracting the pulse that is of interest in earthquake engineering.

In Figure 5, the wavelet $\psi(t)$ is a type-C_1 pulse (Makris and Chang, 2000). Type-C_n pulses can approximate n cycles in the displacement history of a ground motion and are defined as

$$\begin{aligned} u_g^{C_n}(t) = &-\frac{1}{(2\pi)^2}\cos(2\pi t+\varphi) \\ &-\frac{1}{2\pi}t\sin(\varphi)+\frac{1}{(2\pi)^2}\cos(\varphi), \\ 0 \le n \le &\left(n+\frac{1}{2}-\frac{\varphi}{\pi}\right)T_p. \end{aligned} \tag{17}$$

In deriving equation (17), the value of the phase angle, φ, is determined by requiring that the ground displacement at the end of the pulse be zero. A type-C_n pulse has duration $(n+\frac{1}{2}-\frac{\varphi}{\pi})T_p$, and the zero displacement requirement at the end of the pulse gives

$$\cos[(2n+1)\pi-\varphi]+[(2n+1)\pi-2\varphi]\sin(\varphi) = 0. \tag{18}$$

The solution of the transcendental equation given by equation (18) gives the value of the phase angle, φ, for a given value of n. For instance, for a type-C_1 pulse ($n = 1$), $\varphi = 0.0697\pi$, whereas for a type-C_2 pulse ($n = 2$), $\varphi = 0.0410\pi$. Later in this paper we examine wavelets that allow for a continuous modulation of the phase.

Baker (2007) computed the continuous wavelet transform of the velocity time history and identified the coefficient $C(S,\Xi)$ with the largest absolute value. The dominant daughter wavelet associated with this value identifies the period and location of the main velocity pulse. The Daubechies wavelet of order 4 was used. In Baker's (2007) work, the dominant wavelet is subtracted from the velocity time history, and the continuous wavelet transform is computed for the residual velocity signal. Again, the next largest absolute value of the wavelet transform of the remaining velocity signal is identified at this step and the same procedure is repeated. Often only one or two repetitions are needed to satisfactorily describe the pulse, but a total of 10 repetitions were performed in Baker's (2007) work to ensure that the pulse is represented in a detailed manner. Finally, in Baker's work, the weighting function, $w(s)$, in the definition of the wavelet transform given by equation (12) is taken without any discussion equal to $1/\sqrt{s}$ ($w(s) = 1/\sqrt{s}$), which enforces that all wavelets, $\psi_{s,\xi}(t) = w(s)\psi(\frac{t-\xi}{s})$, at every scale, s, have the same energy (see equation 13) . Furthermore, Baker (2007) utilized the default built-in wavelet functions of the 2007 MATLAB Wavelet Toolbox in which wavelets at all scales are normalized to

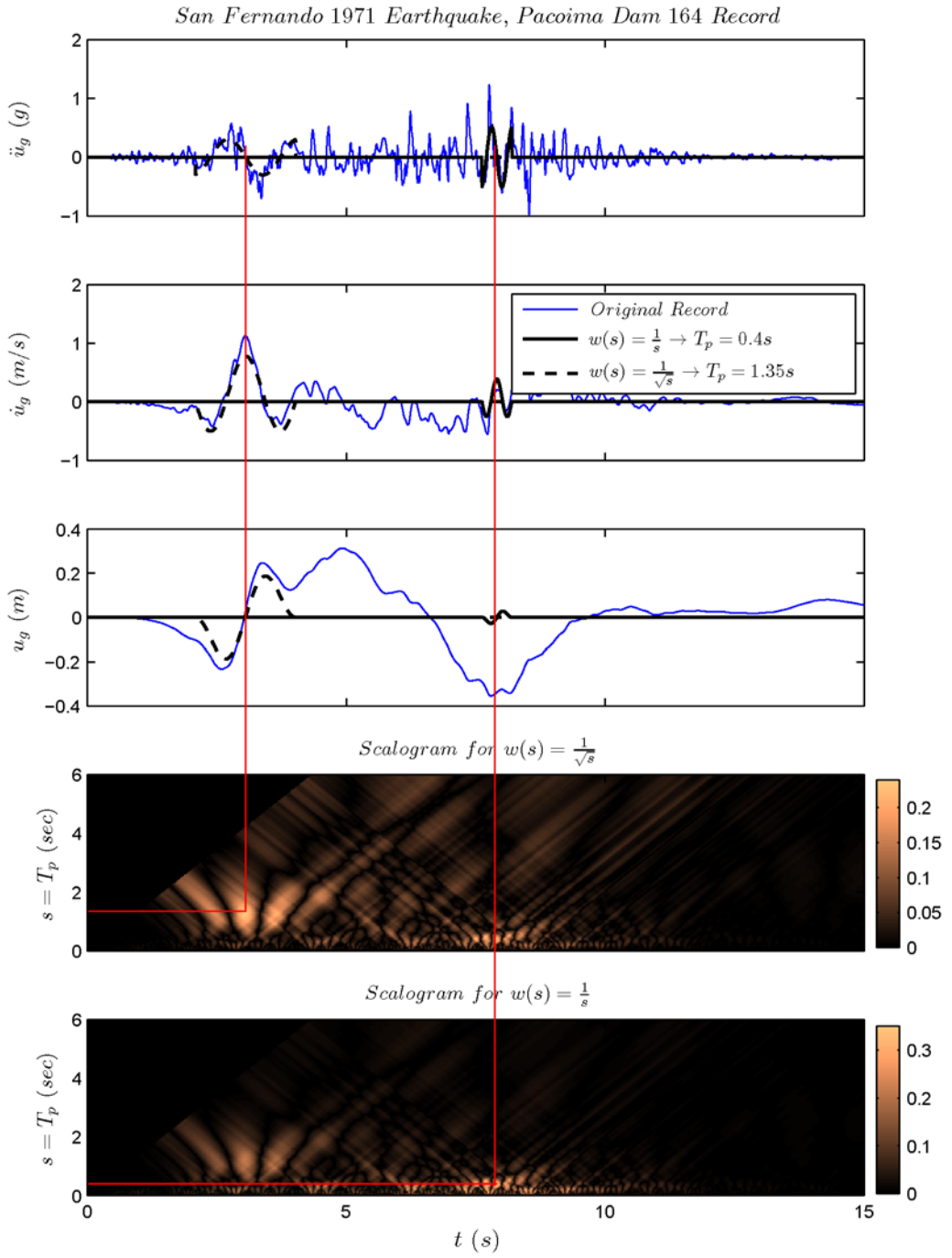

Figure 5. The distinct local pulses captured with wavelet analysis and the role of the power law of the weighting function, $w(s)$. The color version of this figure is available only in the electronic edition.

have unit energy ($E = \int_{-\infty}^{\infty} |\psi_{s,\xi}(t)|^2 dt = 1$, see equation 11). The implications of $w(s) = 1/\sqrt{s}$ and $E = 1$ are explained in detail in Appendix A.

Selection of the Best-Matching Wavelet

The question that arises is which wavelet best matches the majority of records so that it can be used with confidence to invariably extract the pulse period and pulse amplitude of any pulselike acceleration record. In addition to the Ricker wavelet (second derivative of the Gaussian distribution introduced by equation 10) and the type-C_1 pulses and type-C_2 pulses introduced by equation (17), this paper examines the performance of two additional wavelets, that of a one-cosine acceleration pulse (forward and back displacement) and that of the derivative of the symmetric Ricker Wavelet (i.e., the third derivative of the Gaussian). Figure 6 summarizes the five candidate wavelets examined. Note that

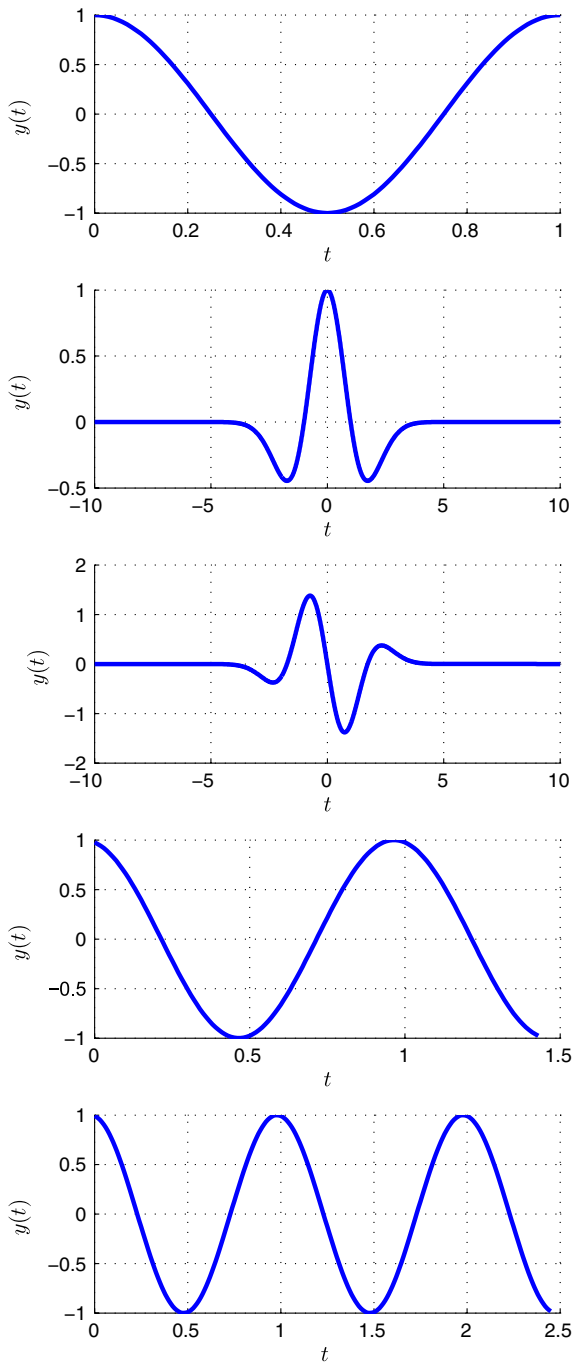

One Cosine
Type B Cyclodial Pulse

$y(t) = cos(2\pi t)$,
$0 < t < 1$

Symmetric Ricker Wavelet
(2^{nd} Derivative of Gaussian, Mexican Hat)

$y(t) = (1 - t^2)e^{\frac{-t^2}{2}}$

Antisymmetric Ricker Wavelet
(3^{rd} Derivative of Gaussian)

$y(t) = te^{\frac{-t^2}{2}}(t^2 - 3)$

Type C1 Cyclodial Pulse

$y(t) = cos(2\pi t + 0.0697\pi)$,
$0 < t < 1.4303$

Type C2 Cyclodial Pulse

$y(t) = cos(2\pi t + 0.0410\pi)$,
$0 < t < 2.459$

Figure 6. Elementary symmetric and antisymmetric wavelets used in this study. The color version of this figure is available only in the electronic edition.

the mathematical expressions appearing in Figure 6 are for the mother wavelets (scale $s = 1$), and this is why the symbol of frequency, f, does not appear in the expressions. Each of these wavelets was used to match, to the greatest extent possible, the 183 records listed in chronological order in Ⓔ Table S1 in the electronic supplement to this paper. As an example, Figure 7 shows the performance of each of the five candidate wavelets listed in Figure 6 (top five graphs) when matching the El Centro Array #5 record from the 1979 Imperial Valley earthquake. The measure used to evaluate the capability of a wavelet to locally match the predominant acceleration pulse (matching index) is the inner product of the extracted mathematical pulse, $\lambda(S, \Xi)\psi_{S,\Xi}(t)$, with the acceleration record, normalized with the energy of the record:

$$e_a = \frac{\int_{-\infty}^{\infty} \ddot{u}_g(t) \cdot \lambda(S, \Xi)\psi_{S,\Xi}(t)dt}{\int_{-\infty}^{\infty} (\ddot{u}_g(t))^2 dt}. \qquad (19)$$

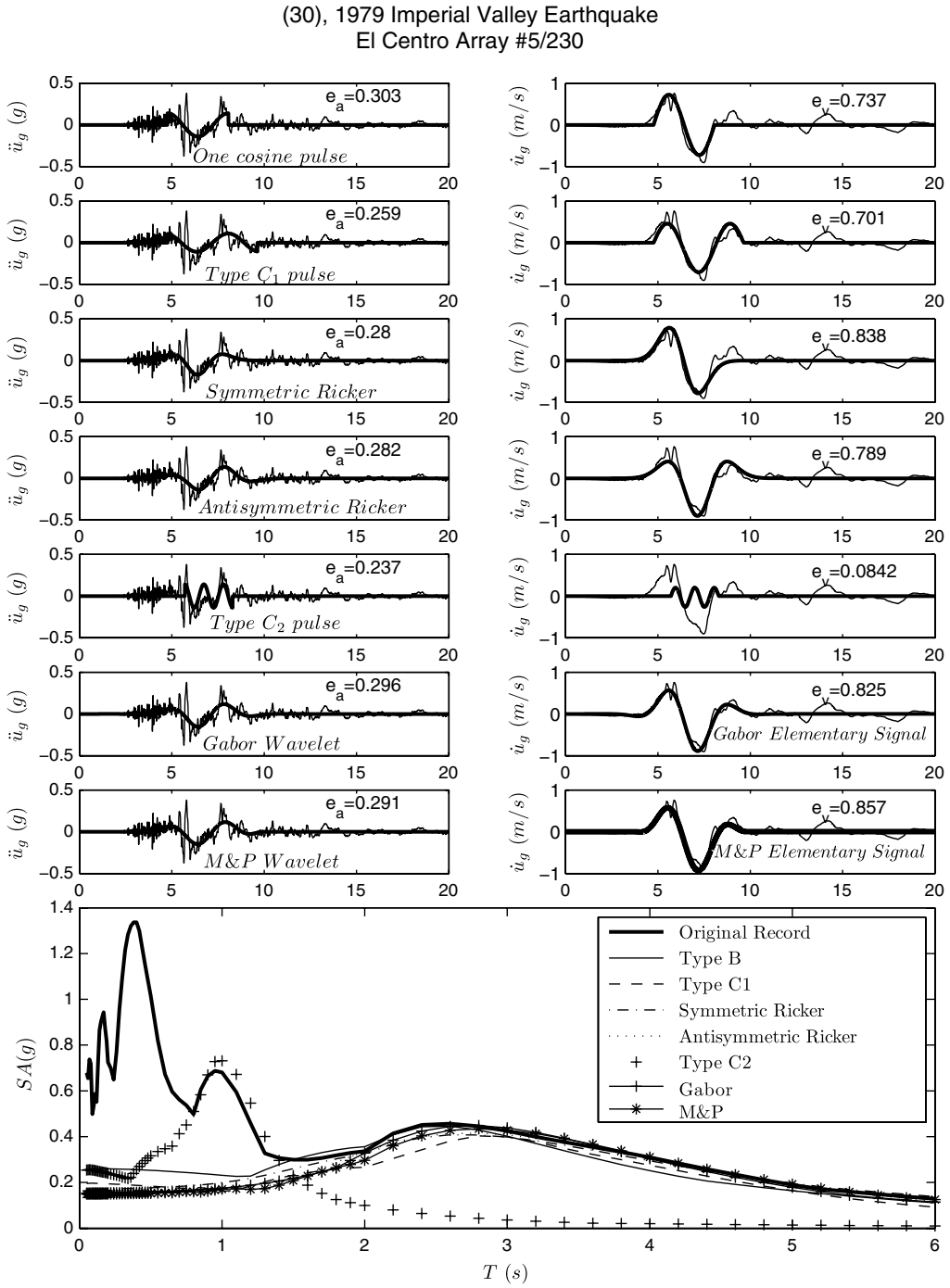

Figure 7. Matching of the acceleration record with various elementary wavelets (left) and the resulting velocity signals (right). In the wavelet transform, all daughter wavelets have the same energy. Bottom: Comparison of the elastic acceleration response spectra with 5% viscous damping.

In Figure 7, the winner of the contest is the one cosine acceleration pulse with $e_a = 0.3030$; whereas, in Figure 8, the best-matching wavelet of the 1992 Erzikan, Turkey, record is the symmetric Ricker wavelet (Mexican Hat wavelet). The scores of the five wavelets appearing in Figure 6 during the contest of best matching all 183 acceleration records are obtained as follows. When matching each record, the wavelet with the highest matching index, e_a, takes 4 points, the second best takes 3 points, the third takes 2 points, the one before last takes one point, and the last one takes zero points. In this way a wavelet that takes many second places may win the contest. The winner of the contest is the antisymmetric C_1 cycloidal pulse with score 449, while very close yet second is the one-cosine acceleration pulse with score 421, which is a symmetric wavelet. Clearly, there is no clear winner because the outcome of the contest depends on the set of ground

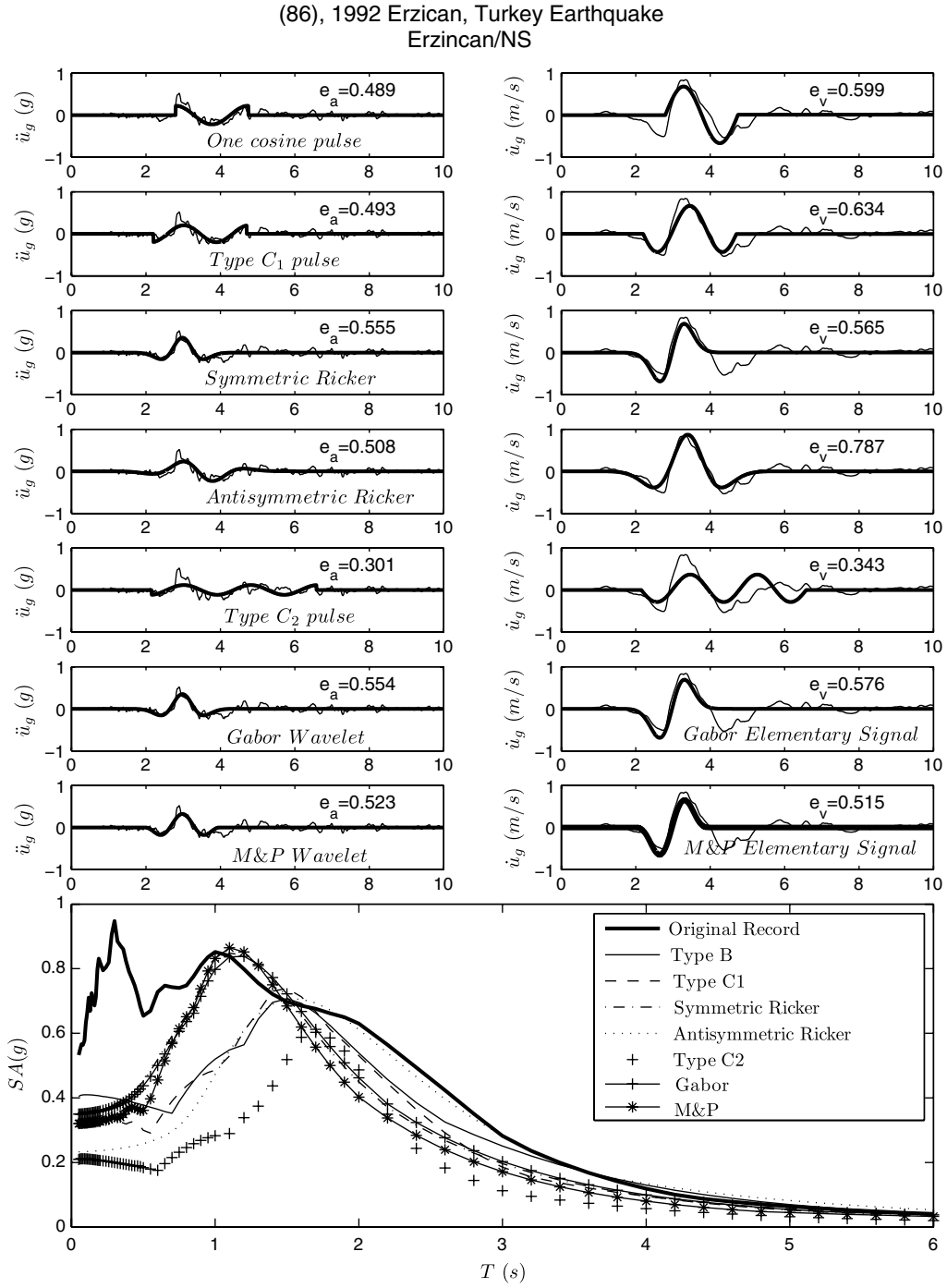

Figure 8. Matching of the acceleration record with various elementary wavelets (left) and the resulting velocity signals (right). In the wavelet transform, all daughter wavelets have same energy. Bottom: Comparison of the elastic acceleration response spectra with 5% viscous damping.

motions, which probably includes more records with antisymmetric coherent pulses than symmetric pulses. The above exercise indicates that in order to satisfy the request of satisfactorily matching the majority of records with a single mother wavelet, this wavelet should allow for a manipulation of its phase, while, at the same time, the number of cycles plays a decisive role in order to achieve a best fit. Accordingly, it becomes apparent that our exercise to identify the best-matching wavelet should incorporate, in addition to the standard translation and dilation-contraction of the wavelet transform, a phase modulation together with an alternation of the oscillatory character (addition of cycles) of the wavelet.

At this point, in addition to the matching index, e_a (subscript a is for acceleration), we define e_v as

$$e_v = \frac{\int_{-\infty}^{\infty} \dot{u}_g(t) \cdot v(t) dt}{\int_{-\infty}^{\infty} (\dot{u}_g(t))^2 dt}, \tag{20}$$

where $v(t)$ is the velocity pulse associated with the extracted acceleration pulse, $\lambda(S, \Xi)\psi_{S,\Xi}(t)$,

$$v(t) = \int \lambda(S, \Xi)\psi_{S,\Xi}(t) dt. \tag{21}$$

The dimensionless quantity, $0 \le e_v \le 1$, given by equation (20), expresses how well the resulting velocity pulse approximates the velocity time history of the record. While our evaluation in selecting the best-matching wavelet uses only the matching index e_a as defined by equation (19), the quantity e_v is involved later in this work in an effort to distinguish pulselike from nonpulselike ground motions.

Extension of the Wavelet Transform by Also Modulating the Phase and the Oscillatory Character of the Elementary Signal

In the classical wavelet transform defined with equation (12), the mother wavelet is subjected to a translation together with a dilation-contraction, $\psi(\frac{t-\xi}{s})$. The dilation-contraction is controlled with the scale parameter s, while the movement of the wavelet along the time axis is controlled with the translation time, ξ. For instance, any daughter wavelet of the symmetric Ricker mother wavelet given by equation (10) assumes the form

$$\psi\left(\frac{t-\xi}{s}\right) = \left[1 - \left(\frac{t-\xi}{s}\right)^2\right] e^{-\frac{1}{2}(\frac{t-\xi}{s})^2}. \tag{22}$$

The need to include four parameters in a mathematical expression of a simple wavelike function that is a good candidate to express the coherent component of a recorded ground motions was presented and addressed by Mavroeidis and Papageorgiou (2003).Without knowing the results of the contest presented in the previous section of this paper, Mavroeidis and Papageorgiou (2003) suggested that a sound analytical model for pulselike records should include four parameters, that is, the pulse duration (or period), the pulse amplitude, the number of cycles, and the phase of the pulse. They identified as the most appropriate analytical expression the Gabor (1946) elementary signal, which they slightly modified to facilitate derivations of closed-form expressions of the spectral characteristics of the signal and response spectra.

One of the earliest and most seminal publications in time-frequency analysis was presented by Gabor (1946). In his 1946 paper, Gabor introduced his elementary signals, which are merely harmonic oscillations modulated by a Gaussian pulse. In his own words, "Each elementary signal can be considered as conveying one 'quantum of information'; therefore, any signal can be expanded in terms of these by a process which includes time analysis and Fourier analysis as extreme cases," a most lucid conception of the wavelet transform more than six decades ago.

The Gabor (1946) elementary signal is defined as

$$g(t) = e^{-(\frac{2\pi f_p}{\gamma})^2 t^2} \cos[2\pi f_p t + \varphi], \tag{23}$$

which is merely the product of a harmonic oscillation with a Gaussian envelope. In equation (23), f_p is the frequency of the harmonic oscillation, φ is the phase angle, and γ is a parameter that controls the oscillation character of the signal. The Gabor wavelike signal given by equation (23) does not have a zero mean; therefore, it cannot be a wavelet within the context of the wavelet transformation. For instance, when the phase φ equals zero, the integral of equation (23) gives

$$\int_{-\infty}^{\infty} e^{-(\frac{2\pi f_p}{\gamma})^2 t^2} \cos[2\pi f_p t + \varphi] dt = \frac{\gamma e^{-\frac{\gamma^2}{4}}}{2\sqrt{\pi} f_p}, \tag{24}$$

which is a finite quantity, not zero.

Nevertheless, the derivative of the Gabor (1946) elementary signal,

$$\frac{dg(t)}{dt} = -\frac{2\pi f_p}{\gamma^2} e^{-(\frac{2\pi f_p}{\gamma})^2 t^2} [\gamma^2 \sin(2\pi f_p t + \varphi) + 4\pi f_p t \cos(2\pi f_p t + \varphi)], \tag{25}$$

is, by construction, a zero-mean signal and is defined in this paper as the Gabor wavelet. According to the notation used in this paper for the wavelet functions, the frequency, f_p, in equation (25) is replaced with the inverse of the scale parameter, $1/s$, while ξ denotes the translation time. Accordingly, the Gabor wavelet is expressed as

$$\psi\left(\frac{t-\xi}{s}, \gamma, \varphi\right) = -\frac{2\pi}{\gamma^2}\frac{1}{s} e^{-(\frac{2\pi}{\gamma})^2 (\frac{t-\xi}{s})^2} \left\{\gamma^2 \sin\left[2\pi\left(\frac{t-\xi}{s}\right) + \varphi\right] + 4\pi\left(\frac{t-\xi}{s}\right) \cos\left[2\pi\left(\frac{t-\xi}{s}\right) + \varphi\right]\right\}. \tag{26}$$

In the expression for the Gabor wavelet given by equation (26), the dilation-contraction is controlled with the parameter s while the movement of the wavelet along the time axis is controlled with translation parameter ξ, the same way as is done in the Ricker wavelet given by equation (22). The novel attraction in the Gabor wavelet given by equation (26) is that, in addition to the dilation-contraction and translation $(\frac{t-\xi}{s})$, the wavelet can be further manipulated by modulating the phase, φ, and the parameter, γ, which controls the oscillatory character (number of half cycles). We can now define the four-parameter wavelet transform as

$$C(s, \xi, \gamma, \varphi) = w(s, \gamma, \varphi) \int_{-\infty}^{\infty} \ddot{u}_g(t) \psi\left(\frac{t-\xi}{s}, \gamma, \varphi\right) dt. \tag{27}$$

The inner product, given by equation (27), is performed repeatedly by scanning not only at all times, ξ, and scales, s, but also by scanning various phases, $\varphi = \{0, \pi/4, \pi/2, 3\pi/4\}$, and various values of the oscillatory nature of the signal $\gamma = \{1.0, 1.5, 2.0, 2.5, 3.0\}$. When needed, more values of φ and γ may be scanned. The quantity $w(s, \gamma, \varphi)$ outside the integral is a weighting function, which is adjusted according to the application.

The values of $s = S$, $\xi = \Xi$, $\gamma = \Gamma$, $\varphi = \Phi$, for which the coefficient $C(s, \xi, \gamma, \varphi) = C(S, \Xi, \Gamma, \Phi)$ reaches its maximum value, offer the scale, location, phase, and number of half cycles of the wavelet $\psi(\frac{t-\xi}{s}, \gamma, \varphi)$ that locally best match the acceleration record, $\ddot{u}_g(t)$. Figure 9 plots the magnitude of the extended wavelet transform, $C(s, \xi, \gamma, \varphi)$, of the El Centro Array #5 acceleration record for various scales as a function of time and four different values of the phase $\varphi = \{0, \pi/4, \pi/2, 3\pi/4\}$ when $\gamma = 3$. The maximum value of the wavelet transform $C(s, \xi, \gamma, \varphi)$ is located at $s = T_p = 3.8$ s and $\varphi = 3\pi/4$.

Figures 7 and 8 (sixth plot from the top) plot the shape of the Gabor wavelet, $\lambda(S, \Xi, \Gamma, \Phi) \cdot w(S, \Gamma, \Phi) \cdot \psi(\frac{t-\Xi}{S}, \Gamma, \Phi)$, where the values ($S$, Ξ, Γ, and Φ) are those that maximize the extended wavelet transform, given by equation (27), in which $\ddot{u}_g(t)$ is the El Centro Array #5 acceleration record from the 1979 Imperial Valley earthquake and the 1992 Erzikan, Turkey, record, respectively. Note that the matching indexes for the Gabor wavelets, $e_a = 0.29635$ in Figure 7 and $e_a = 0.55384$ in Figure 8, are high, yet they rank at the third place. The multiplication coefficient, $\lambda(S, \Xi, \Gamma, \Phi)$, which dictates how much the best-matching generalized wavelet $w(S, \Gamma, \Phi) \cdot \psi_{S,\Xi,\Gamma,\Phi}(t)$ needs to be amplified to best approximate the energetic acceleration pulse, is obtained with an analysis similar to the one presented in Appendix A:

$$\lambda(S, \Xi, \Gamma, \Phi) = \frac{C(S, \Xi, \Gamma, \Phi)}{w^2(S, \Gamma, \Phi) \cdot S \cdot E(\Gamma, \Phi)}. \tag{28}$$

The elementary signal proposed by Mavroeidis and Papageorgiou (2003) to approximate velocity pulses is a slight modification of the Gabor signal given by equation (23), where the Gaussian envelope has been replaced by an elevated cosine function:

$$v(t) = \frac{1}{2}\left[1 + \cos\left(\frac{2\pi f_p}{\gamma} t\right)\right] \cos(2\pi f_p t + \varphi), \quad -\frac{\gamma}{2f_p} \le t \le \frac{\gamma}{2f_p}. \tag{29}$$

Clearly the wavelike signal given by equation (29) does not always have a zero mean; therefore, it cannot be a wavelet within the context of wavelet transform. Nevertheless, the time derivative of the elementary velocity signal given by equation (30):

$$\frac{dv(t)}{dt} = -\frac{\pi f_p}{\gamma}\left\{\sin\left(\frac{2\pi f_p}{\gamma} t\right)\cos(2\pi f_p t + \varphi) + \gamma \sin(2\pi f_p t + \varphi)\left[1 + \cos\left(\frac{2\pi f_p}{\gamma} t\right)\right]\right\}, \quad -\frac{\gamma}{2f_p} \le t \le \frac{\gamma}{2f_p}, \tag{30}$$

which is, by construction, a zero-mean signal and is defined in this paper as the Mavroeidis and Papageorgiou (M&P) wavelet. After replacing the oscillatory frequency, f_p, with the inverse of the scale parameter, the M&P wavelet is defined as

$$\psi\left(\frac{t-\xi}{s}, \gamma, \varphi\right) = \left\{\sin\left[\frac{2\pi}{s\gamma}(t-\xi)\right]\cos\left[\frac{2\pi}{s}(t-\xi) + \varphi\right] + \gamma \sin\left[\frac{2\pi}{s}(t-\xi) + \varphi\right]\right\} \times \left\{1 + \cos\left[\frac{2\pi}{\gamma s}(t-\xi)\right]\right\}, \quad \xi - \frac{\gamma}{2f_p} \le t \le \xi + \frac{\gamma}{2f_p}. \tag{31}$$

It is worth noting that the mathematical structure of both the Gabor and the M&P elementary signals forces us to conduct the extended wavelet transform on the acceleration records (not the velocity records), given that only the time derivatives of the elementary signals are wavelets within the context of the wavelet transform. Clearly, when selecting the appropriate weighting function, $w(s, \gamma, \varphi)$, the wavelet transform on the acceleration records proposed in this paper leads to the velocity pulses presented by Mavroeidis and Papageorgiou (2003) and Baker (2007), yet, most importantly, the coherence of the ground motion extracted with this work is directly related to the inertia effects on structures, given that it originates from the acceleration records.

The last time-history plot on the left of Figures 7 and 8 is denoted with a heavy line the shape of the M&P wavelet (equation 31) where the values of $s = S$, $\xi = \Xi$, $\gamma = \Gamma$, and $\varphi = \Phi$ are those that maximize the extended wavelet transform given by equation (27), in which $\ddot{u}_g(t)$ is, respectively, the 1979 El Centro Array #5 and the 1992 Erzikan, Turkey, acceleration records. Note that the matching index for the M&P wavelet is $e_a = 0.2963$ in Figure 7 and $e_a = 0.5538$ in Figure 8, and they rank very high, yet second in each Figure. In Figure 7, the M&P wavelet ranks slightly behind the one-cosine acceleration pulse; whereas, in Figure 8, the M&P wavelet ranks slightly behind the symmetric Ricker wavelet.

In order to address the question of which wavelet best matches the majority of records, the scores of the seven wavelets under examination (five wavelets appearing in Figure 6 plus the Gabor and M&P wavelets defined by equations 26 and 31) are obtained following the protocol defined in the previous section. When matching each record, the wavelet with the highest matching index, e_a, takes 6 points, the second best takes 5 points, all the way to the last

matching index, which takes zero points. Figure 10 portrays the scores of all seven wavelets of interest in the form of a histogram. The M&P wavelet ranks first ahead of the Gabor wavelet, while the other five wavelets listed in Figure 6, which do not allow for phase modulation and manipulation of their oscillatory character, fall far behind. In order to emphasize the significant advantage of the extended wavelet transform introduced in this paper, Figure 11 shows the scores of the five wavelets listed in Figure 6 when competing only against the Gabor wavelet (top) or only against the M&P wavelet (bottom).

Given that the M&P wavelet (equation 31) gains the highest score in both contests shown in Figure 10 and Figure 11 (bottom), the M&P wavelet is selected as the best-matching wavelet and is the one used to process the database of the 183 acceleration records, most of which are intentionally pulselike (Baker, 2007). While the proposed methodology can extract the most energetic acceleration pulse for a given expression of the weighting function, $w(s)$, our study examines mostly pulselike ground motions in order to show the efficiency of the proposed method to extract well-known pulses that have been identified in the literature.

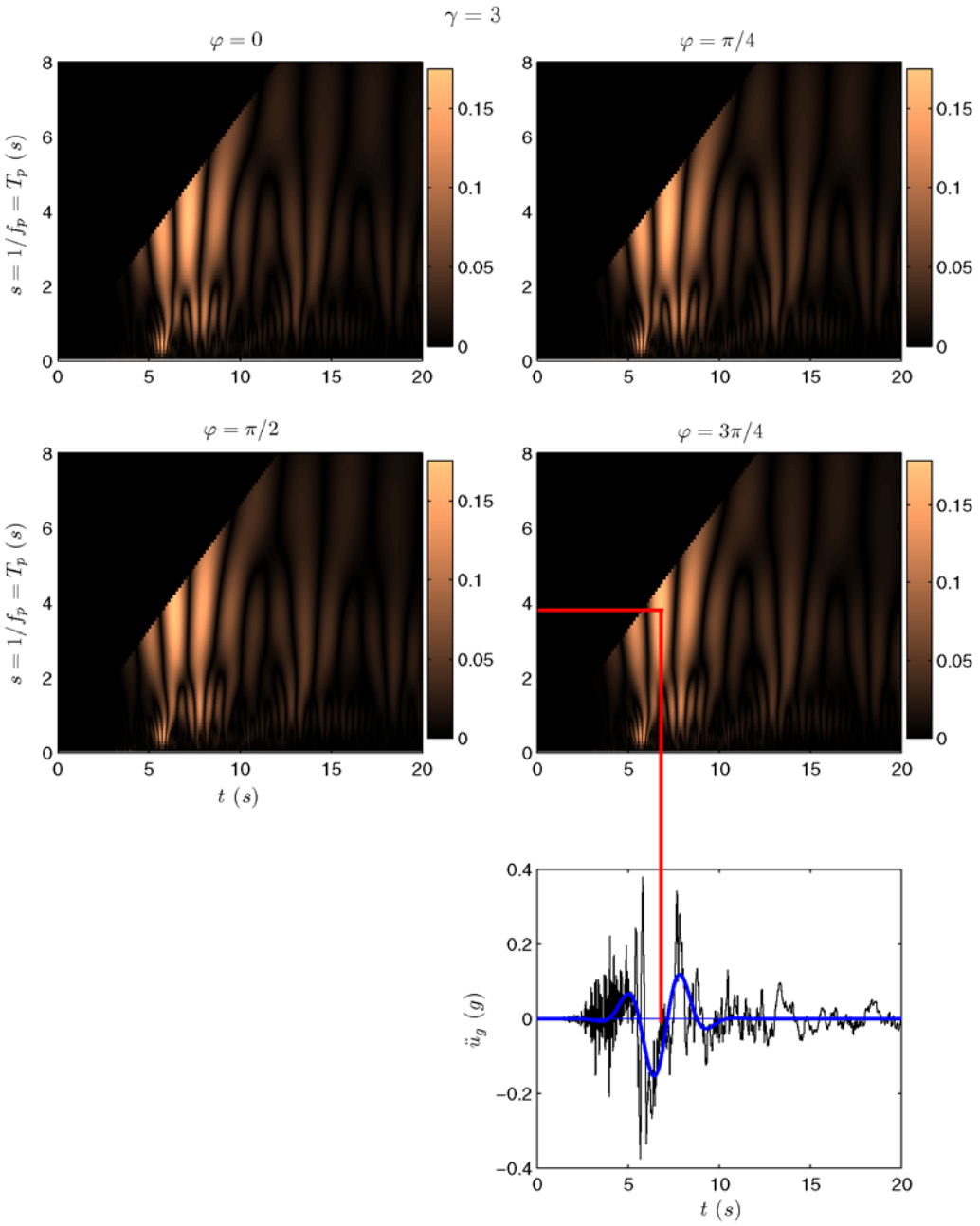

Figure 9. Scalograms of the extended wavelet transform defined by equation (27) exercised on the El Centro Array #5 acceleration record from the 1979 Imperial Valley earthquake with the Gabor wavelet ($\gamma = 3$). The maximum value of the wavelet transform is located at $s = T_p = 3.8$ s, $\gamma = 3$, and $\varphi = 3\pi/4$. The color version of this figure is available only in the electronic edition.

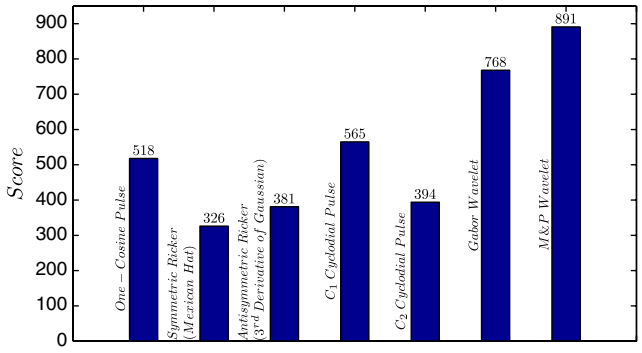

Figure 10. Scores of the seven wavelets of interest in this paper from the contest of best matching the 183 records listed in Ⓔ Table S1 in the electronic supplement to this paper. The high scores of the M&P and the Gabor wavelets are due to their ability to modulate their phase and oscillatory character as implemented with the extended wavelet transform proposed in this paper. The color version of this figure is available only in the electronic edition.

Time Scales and Length Scales of Strong Ground Motions

The parameters of the M&P wavelets that maximize the extended wavelet transform of the strong ground motions listed in Ⓔ Table S1 in the electronic supplement to this paper are extracted by setting the weighting function, $w(s, \gamma, \varphi)$, in equation (27) such that all daughter wavelets have (1) the same area, (2) the same energy, and (3) the same amplitude. For instance, for the M&P wavelet defined by equation (31), the same energy requirement gives

$$w(s,\gamma,\varphi) = \frac{1}{\sqrt{\frac{1}{8}s\left[2\gamma + 6\gamma^3 + \frac{\cos(2\varphi)\sin(2\pi\gamma)}{\pi(1-4\gamma^2)}\right]}}. \qquad (32)$$

In several occasions, even the same energy requirement on the wavelet transform results in energetic acceleration pulses that do not correspond to the long velocity pulses derived visually. For instance, Figure 12 shows the performance of each of the seven wavelets examined in this paper when matching the Parachute Test Site, 225 records from the 1981 Westmorland earthquake. With the same energy requirement, the first two wavelets capture a long-duration pulse that becomes apparent in the velocity time histories shown on the right of Figure 12. On the other hand, the same energy requirement on the next five wavelets (from the symmetric Ricker to the M&P wavelet) extracts a higher frequency pulse, not the longer period pulse that dominates the velocity record. Note that the higher score goes to the M&P wavelet, $e_a = 0.1687$. The acceleration spectra of a linear SDOF structure shown at the bottom of Figure 12 indicates that the shorter period acceleration pulse ($T_p = 0.6$ s) extracted with the last five wavelets (from symmetric Ricker to the M&P wavelet) is most relevant to structures with a fundamental period equal to 0.6 s (3–6-story buildings), while the longer period acceleration pulse extracted with the first two wavelets (one-cosine and type-C_1 pulses) is most relevant to the structures with fundamental period above 3 s (e.g., seismic isolated structures and longer period bridges).

In order for the last five wavelets (from the symmetric Ricker to the M&P wavelet) to capture the longer acceleration pulse that dominates the velocity signal, the same energy requirement needs to be replaced by the same amplitude requirement (a weighting function that suppresses the longer scales less), as shown in Figure 13.

In conclusion, in any given record, different pulses may be extracted with each weighting function, $w(s)$. For instance, the parameters of the pulses that result in the maximum pseudoacceleration of two elastic SDOF oscillators with natural periods, $T_0 = 0.5$ s and $T_0 = 2.5$ s, are marked with bold face in Ⓔ Table S1 in the electronic supplement to this paper.

In calculating the maximum pseudoacceleration response, the closed-form expressions offered in the paper by Mavroeidis *et al.* (2004) are used. Similarly, using the charts of Figure 7 of Mavroeidis *et al.* (2004), one can determine which pulse is the most destructive to a given inelastic SDOF.

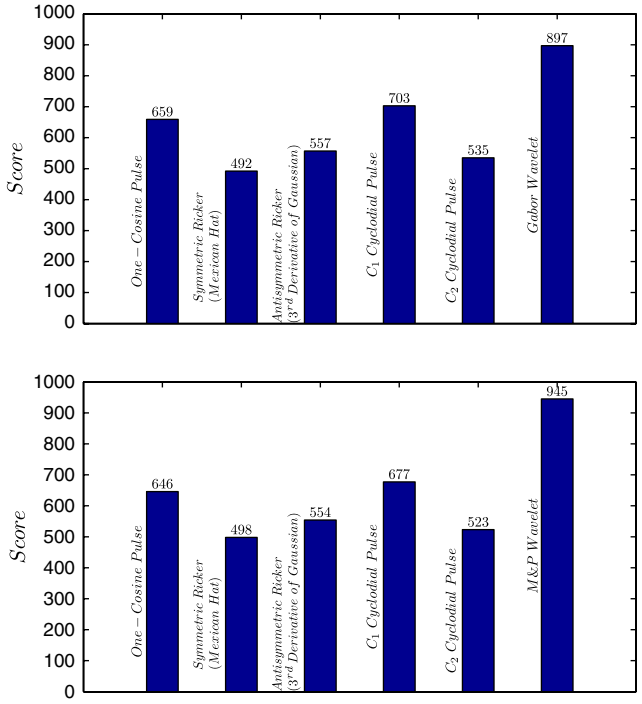

Figure 11. Comparison of the two parameter wavelets listed in Figure 6 with the Gabor (top) and the M&P (bottom) four-parameter wavelets from the contest of best matching the 183 records listed in Ⓔ Table S1 in the electronic supplement to this paper. The color version of this figure is available only in the electronic edition.

Determination of the Significance of the Extracted Pulse—Classification of Motions as Pulselike

The initial motivation of Bertero *et al.* (1978) to direct the attention of engineers to coherent acceleration pulses and

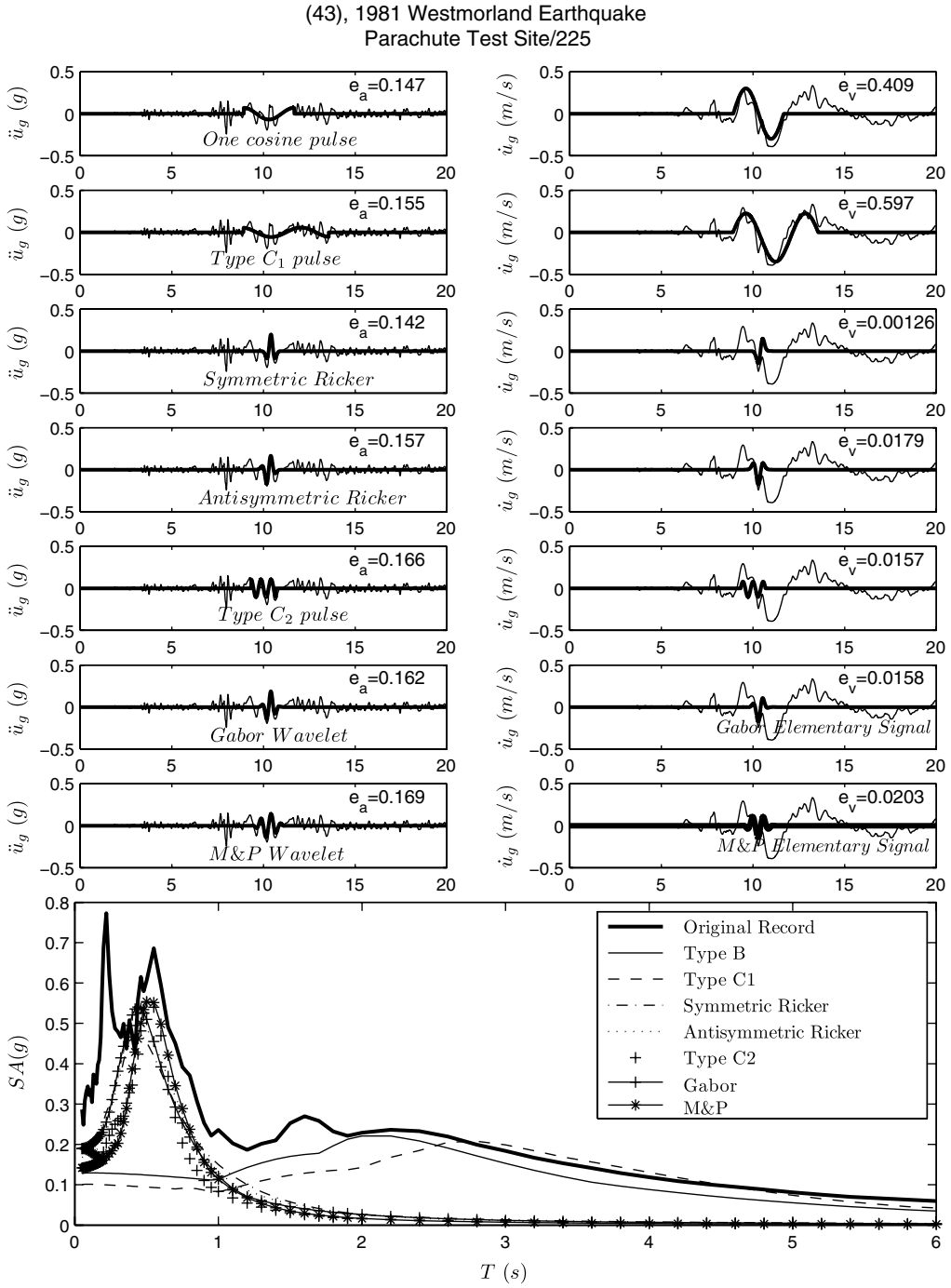

Figure 12. Matching of the acceleration record with various elementary wavelets (left) and the resulting velocity signals (right). In the wavelet transform, all daughter wavelets have the same energy. Bottom: Comparison of the elastic acceleration response spectra with 5% viscous damping.

our continuing interest in identifying and characterizing them are mainly motivated from the need to estimate inelastic deformation demands on structures. As an example, equation (8) offers estimates of peak inelastic deformations of a bilinear structural idealization as a function of the period and amplitude of the dominant acceleration pulse.

Clearly, the more a ground motion is pulselike, the more the results from mastercurves like the one expressed by equation (8) are dependable. Accordingly, some indicator is needed to indicate to what extent a recorded ground motion is pulselike. Efforts to classify ground motions have been presented in the past. Baker (2007), after a preliminary visual classification of the velocity records, proceeds by proposing a pulse indicator that is a function of a PGV ratio and an energy ratio. Clearly, both the PGV ratio and the energy ratio involve information solely from the velocity time history, and

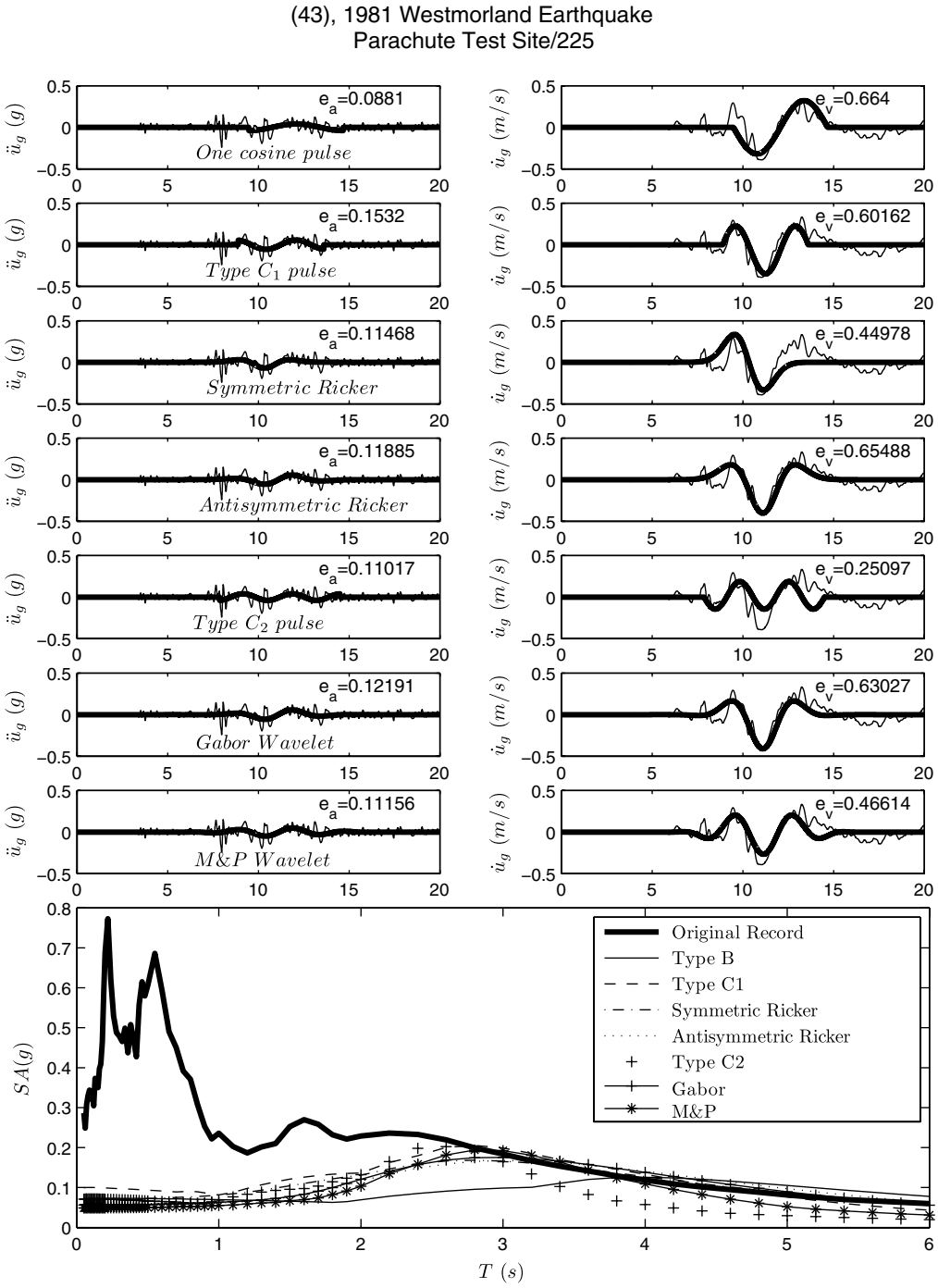

Figure 13. Matching of the acceleration record with various wavelets (left) and the resulting velocity signals (right). In the wavelet transform, all daughter wavelets have the same amplitude. Bottom: Comparison of the elastic acceleration response spectra with 5% viscous damping.

therefore Baker's pulse indicator does not have the ability to identify shorter duration pulses that occasionally govern to a great extent the response of structures as shown in Figure 2. While Baker (2007) recognized that on several occasions in his analysis, the pulse period obtained from his wavelet analysis differed significantly from the pulse period obtained from the velocity spectrum analysis, no information was offered as to what extent the pulses that he identified with a high pulse indicator value (PI > 0.85) impose force and displacement demands on structures comparable to those imposed by the recorded motion. This is an issue of significant engineering interest that deserves further investigation.

We return to Figure 2, where the shorter duration overriding pulse with period $T_p = 1.75$ s is shown to be of major engineering interest because it is responsible for most of the base shear and peak deformation of elastic and inelastic

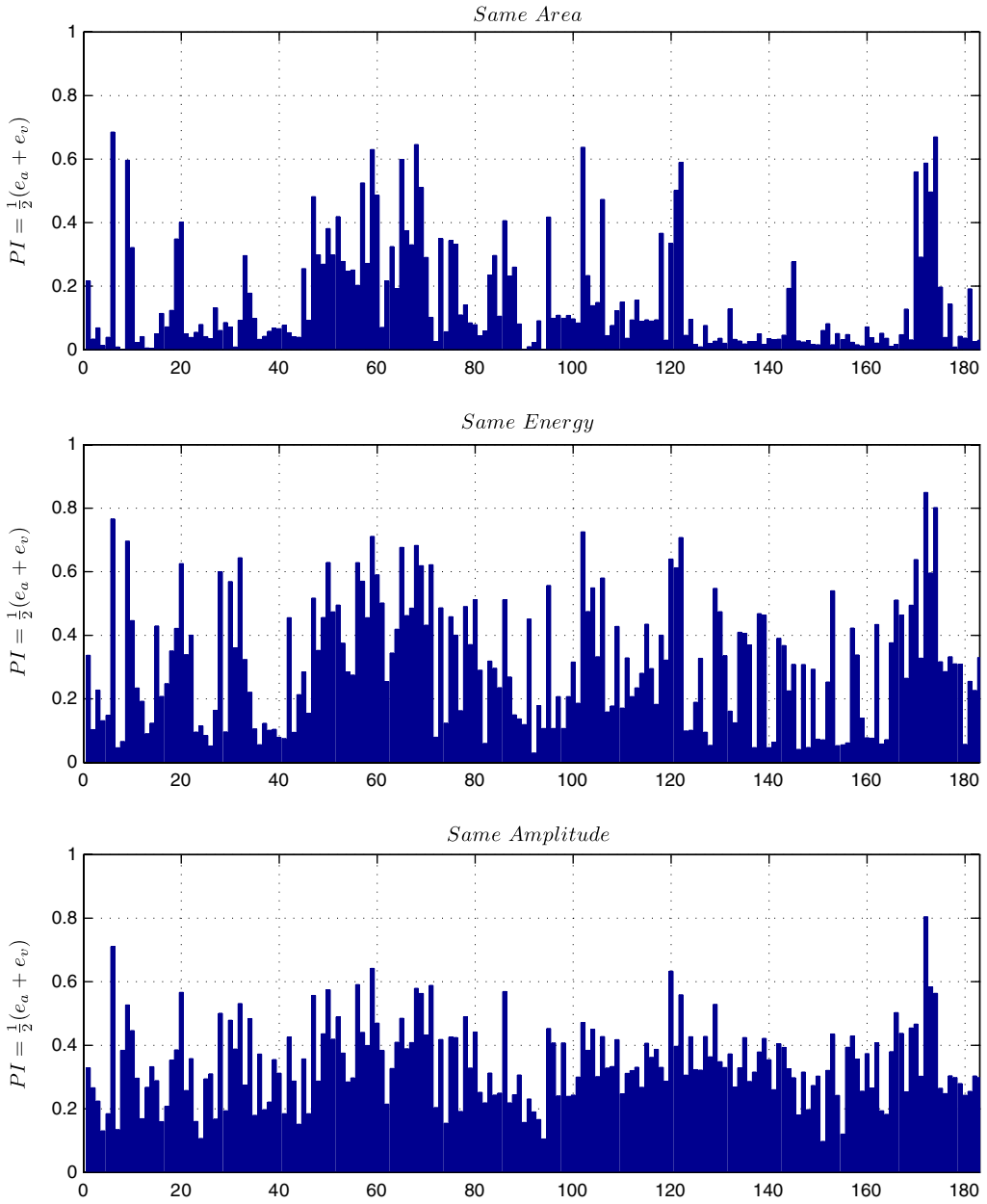

Figure 14. Values of the proposed pulse indicator from the 183 records listed in Ⓔ Table S1 in the electronic supplement to this paper when equal-area (top), equal-energy (center), and equal-amplitude (bottom) wavelets are used. The color version of this figure is available only in the electronic edition.

structures. For this shorter duration pulse, which is extracted with the proposed wavelet analysis with an equal energy weighting function, its matching index, e_a, as defined by equation (19), is $e_a = 0.548$, a value that indicates that the short acceleration pulse is strongly correlated with the acceleration record. This strong correlation is confirmed in a most convincing way by the response spectra shown in the lower part of Figure 2. Specifically, for the sliding oscillator ($\mu = 5\%$ and 10%), the acceleration and displacement spectra are almost identical for structural periods, T_s, up to 5.0 s, whereas, for the elastic oscillator ($\xi = 5\%$), the same is true for structural periods T_s up to 3.0 s. On the other hand, the quantity e_v, which expresses the correlation between the associated short velocity pulse and the velocity record, as defined by equation (20), has a feeble value, $e_v = 0.0693$. Nevertheless, this feeble correlation in the velocity histories will not lessen the important engineering significance of the short duration acceleration pulse with $T_p = 1.75$ s.

At the same time, one should not neglect the presence of the 9-s-long velocity pulse that is associated with the near-source effects and is extracted with the proposed wavelet analysis with an equal-amplitude weighting function.

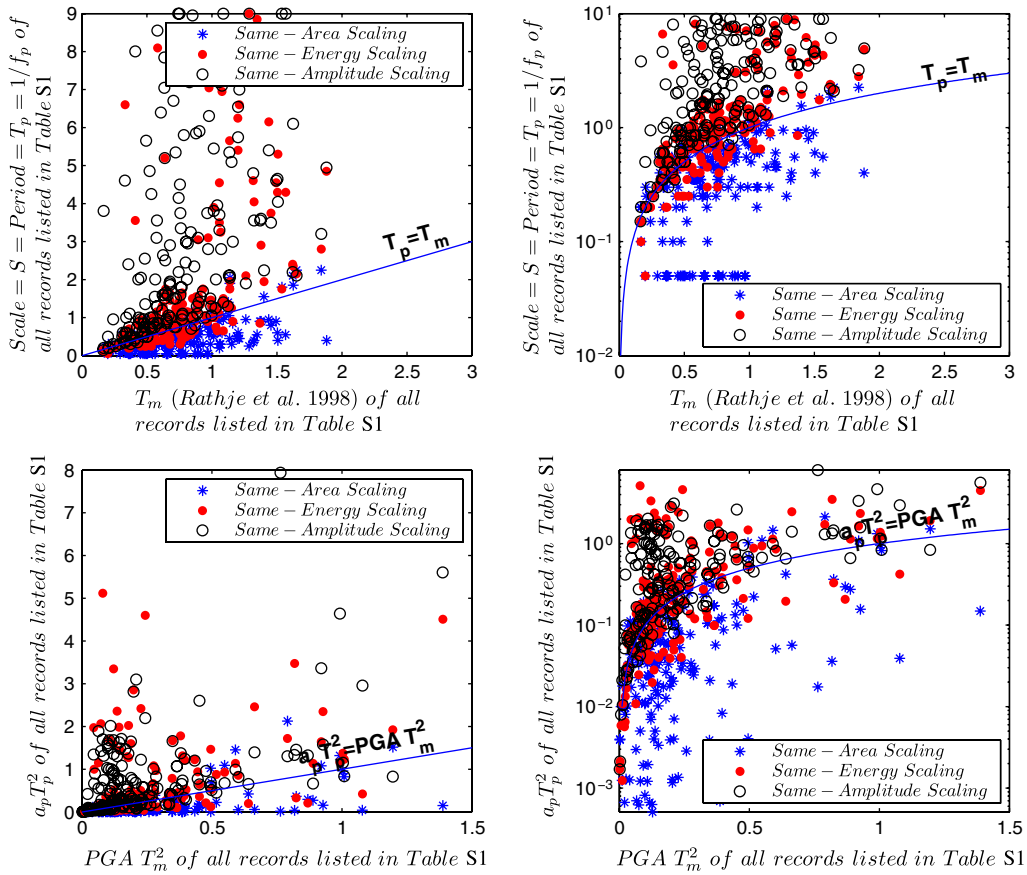

Figure 15. Top: Comparison of the length scale $T_p = S$ as results from the extended wavelet transform of the records when convolved with the M&P wavelets together with the period T_m (Rathje *et al.*, 1998). Bottom: Comparison of the corresponding energetic length scales, $a_p T_p^2$, resulting from the M&P wavelets together with the length scale $L_e = \text{PGA} \cdot T_m^2$. Ⓔ Table S1 is available in the electronic supplement to this paper. The color version of this figure is available only in the electronic edition.

The effects of the long-period pulse can be noted in the spectra of the elastic oscillator ($\xi = 5\%$) for values of the structural periods $T_s \geq 6.0$ s. Interestingly, the effect of the 9-s long acceleration pulse, which results in the distinguishable long-velocity pulse with PGV of the order of 1.0 m/s, is not notable in the sliding oscillators ($\mu = 5\%$ and $\mu = 10\%$) because the peak acceleration associated with the long-velocity pulse is too feeble to initiate sliding. The matching coefficient, e_a, of the long acceleration pulse (which has been extracted with the proposed method by processing only the acceleration record) is relatively small ($e_a = 0.101$), whereas the correlation of the velocity histories is strong with a value of $e_v = 0.495$. From the above discussion, it becomes clear that depending on the properties of the structural system, either the shorter duration or the longer duration pulses may be of engineering interest. Accordingly, as a simple pulse indicator (PI), we define

$$\text{PI} = \frac{1}{2}(e_a + e_v). \tag{33}$$

As an example for the short 1.75-s period acceleration pulse extracted with the equal energy weighting function, the following is true: $\text{PI} = \frac{1}{2}(0.548 + 0.0693) = 0.309$; while for the long 9-s period acceleration pulse extracted with the equal-amplitude weighting function, the following is true: $\text{PI} = \frac{1}{2}(0.101 + 0.495) = 0.298$. Accordingly, Figure 2 indicates that a value of $\text{PI} \geq 0.3$ identifies coherent pulses that impose displacement and force demands on structures (in the corresponding period range) comparable to the demands imposed by the recorded motion. Consequently, a value of $\text{PI} \geq 0.3$ is enough to classify the motion as pulselike.

Figure 14 plots the values of the pulse indicator $\text{PI} = \frac{1}{2}(e_a + e_v)$ for all the 183 records (Ⓔ Table S1 in the electronic supplement to this paper) when equal-area (top), equal-energy (center), and equal-amplitude (bottom) wavelets are used in the proposed extended wavelet transform. These values appear for each motion and each analysis in Ⓔ Table S1 (available in the electronic supplement to this paper). Based on the results for the PI associated with Figure 2 (Ⓔ record 145 in Table S1 in the electronic supplement to this paper), one may classify a motion with a pulse indicator $\text{PI} > 0.30$ as pulselike. In this case, 124 out of 183 motions that we used are classified as pulselike.

Nevertheless, it is emphasized that the issue of classifying a ground motion as pulselike hinges upon the ability of the extracted pulse to impose force and displacement

demands comparable to those imposed by the recorded motion. This is a delicate issue, in particular when dealing with inelastic structures, that deserves further investigation.

Comparison with the Mean Period T_m

The challenge to extract a representative time scale of an earthquake is not new. About a decade ago Rathje *et al.* (1998) examined three popular frequency content parameters and concluded that the mean period,

$$T_m = \frac{\sum_j C_j^2 \frac{1}{f_j}}{\sum_j C_j^2} \quad \text{for } 0.25 \text{ Hz} \le f_j \le 20 \text{ Hz}, \tag{34}$$

appears to be the best simplified time-scale characterization parameter. In equation (34), C_j equals Fourier amplitudes of the entire acceleration record, and f_j equals discrete Fourier transform frequencies between 0.25 Hz and 20 Hz. Figure 15 plots along the horizontal axis the computed mean period, T_m, of the earthquake records listed in Ⓔ Table S1 in the electronic supplement to this paper, and on the vertical axis, the corresponding periods of the records extracted with the M&P wavelets when the weighting function in the extended wavelet transform enforces that all daughter wavelets have (1) the same area, (2) the same energy, and (3) the same amplitude. Figure 15 indicates that when the same-area scaling is selected (stars) in the extended wavelet transform (suppression of the long periods), the extracted pulses are mostly short period with pulse periods below the values of T_m, as expressed by equation (34). When the same energy scaling is selected (dark circles), the extracted pulses have pulse periods close to the values of T_m approximately up to values of $T_p = 1$ s, and beyond this value, the pulses extracted with the wavelet transform have pulse periods much larger than T_m. Finally, when the same amplitude scaling is selected (empty circles) in the extended wavelet transform (accentuation of large periods), the extracted pulses consistently have periods larger than those predicted by T_m.

Conclusions

In this paper we developed and validated a mathematically formal and objective procedure to extract the characteristic time scales and length scales of the most energetic acceleration pulses of strong ground motions. The procedure uses wavelet analysis to identify and approximate energetic acceleration pulses (not velocity pulses). The study shows that the weighting function in the definition of the wavelet transform has a dominant role in extracting a specific pulse. For instance, longer pulses, which are often detected visually in the velocity records (and have attracted the attention of Mavroeidis and Papageorgiou (2003) and Baker (2007) among others), can be systematically captured with the wavelet transform of the acceleration records by implementing a weighting function, $w(s)$, that does not suppress the long periods, such as the equal-amplitude weighting function. On the other hand, shorter duration distinguishable pulses that may have significant engineering interest and that occasionally override the long-duration pulses are captured with the wavelet transform by implementing a faster decaying weighting function, $w(s)$.

The capability of several popular symmetric and antisymmetric wavelets to locally match the energetic acceleration pulse is examined, and it is concluded that the exercise to identify the best-matching wavelet shall incorporate, in addition to the standard translation and dilation-contraction of the traditional wavelet transform, a phase modulation together with a manipulation of the oscillatory character (addition of cycles) of the wavelet. This need leads to the extension of the wavelet transform to a more general wavelet transform during which the mother wavelet is subjected to the four functions just mentioned.

The paper examines the performance of two similar elementary signals, the seminal elementary signal proposed by Gabor (1946) and its variation proposed by Mavroeidis and Papageorgiou (2003), which in addition to a period (scale) parameter and an amplitude parameter, include a phase parameter, φ, and an oscillatory character parameter γ. The time derivatives of these elementary signals satisfy the conditions for a wavelike function to be a wavelet and are defined as the Gabor and the M&P wavelets.

The paper examines the capability of the Gabor and M&P wavelets to locally match the energetic acceleration pulse of 183 strong ground motions, and it shows that the performance of the proposed extended wavelet transform, which convolves the acceleration record with the four-parameter wavelets described in the text, outshines the performance of the traditional wavelet transform, which convolves the acceleration record with any two-parameter wavelet.

Finally, the paper compares the resulting time scales of the 183 records examined with the mean period that was proposed by Rathje *et al.* (1998) as a dependable time-scale characterization parameter of an acceleration record. When the same-area scaling is selected (stars, Fig. 15) in the extended wavelet transform (suppression of the long-periods), the extracted pulses are mostly short-period with pulse periods below the values of T_m as expressed by equation (34). When the same energy scaling is selected (dark circles, Fig. 15), the extracted pulses have pulse periods close to the values of T_m approximately up to values of $T_p = 1$ s, and beyond this value, the pulses extracted with the wavelet transform have pulse periods much larger than T_m. Finally, when the same amplitude scaling is selected (empty circles, Fig. 15) in the extended wavelet transform (accentuation of large periods), the extracted pulses consistently have periods larger than those predicted by T_m.

Data and Resources

The earthquake records listed in Ⓔ Table S1 in the electronic supplement to this paper were downloaded from

1. http://peer.berkeley.edu/smcat (last accessed September 2010);
2. http://mceer.buffalo.edu/research/Reconnaissance/LAquila4-06-09/Ground_Motion_Records.asp (last accessed September 2010);
3. http://smbase.itsak.gr/ (last accessed September 2010).

All the computations, numerical analysis, and plotting have been computed with the software MATLAB (2007). http://www.mathworks.com/ (last accessed September 2010).

Acknowledgments

Partial financial support for this study has been provided to the first author by the Alexander S. Onassis Public Benefit Foundation.

References

Addison, P. S. (2002) *The Illustrated Wavelet Transform Handbook* Institute of Physics Handbook, London.

Alavi, B., and H. Krawinkler (2001). Effects of near-fault ground motions on frame structures, *John A. Blume Earthquake Engineering Center Rept. No. 138*, Stanford University.

Baker, W.J. (2007). Quantitative classification of near fault ground motions using wavelet analysis, *Bull. Seismol. Soc. Am.* **97,** 1486–1501.

Bertero, V. V., J. C. Anderson, H. Krawinkler, and E. Miranda (1991). Design guidelines for ductility and drift limits, Rept. No. EERC/UCB-91/15, Earthquake Engineering Research Center, University of California, Berkeley, California,

Bertero, V. V., S. A. Mahin, and R. A. Herrera (1978). Aseismic design implications of near-fault San Fernando earthquake records, *Earthq. Eng. Struct. Dynam.* **6,** 31–42.

Chopra, A. K., and C. Chintanapakdee (2004). Inelastic deformation ratios for design and evaluation of structures: Single-degree-of-freedom bilinear systems. *J. Struct. Eng., ASCE* **130,** No. 9, 1309–1319.

Daubechies, I. (1992). Ten lectures on wavelets, *CBMS-NSF Regional Conference Series in Applied Mathematics*, SIAM, Philadelphia, Ch. 3.

Gabor, D. (1946). Theory of communication. I. The analysis of information, *IEEE* **93,** 429–441.

Hall, J. F., T. H. Heaton, M. W. Halling, and D. J. Wald (1995). Near source ground motion and its effects on flexible buildings, *Earthq. Spectra* **11,** 569–605.

Housner, G. W., and D. E. Hudson (1959). *Applied Mechanics/Dynamics*, Van Nostrand, Princeton, New Jersey.

Karavassilis, T. L., N. Makris, N. Bazeos, and D. E. Beskos (2010). Dimensional response analysis of multi-storey regular steel MRF subjected to pulse-like earthquake ground motions, *J. Struct. Eng. (ASCE)* **136,** 8, 921–932.

Langhaar, H. L. (1951). *Dimensional Analysis and Theory of Models*, Wiley, New York.

Loh, C.-H., Z.-K. Lee, T.-C. Wu, and S.-Y. Peng (2000). Ground motion characteristics of the Chi-Chi earthquake of 21 September 1999, *Earthq. Eng. Struct. Dynam.* **29,** 867–897.

Ma, K.-F., S.-J. Mori, and S. B. Yu (2001). Spatial and temporal distribution for the 1999 Chi-Chi, Taiwan, earthquake, *Bull. Seismol. Soc. Am.* **91,** 1069–1087.

Makris, N. (1997). Rigidity-plasticity-viscosity: Can electrorheological dampers protect base-isolated structures from near-source ground motions? *Earthq. Eng. Struct. Dyn.* **26,** 571–591.

Makris, N., and C. J. Black (2004a). Dimensional analysis of rigid-plastic and elastoplastic structures under pulse-type excitations, *J. Eng. Mech.* **130,** 1006–1018.

Makris, N., and C. J. Black (2004b). Dimensional analysis of bilinear oscillators under pulse-type excitations, *J. Eng. Mech.* **130,** 1019–1031.

Makris, N., and C. Black (2004c). Evaluation of peak ground velocity as a "good" intensity measure for near-source ground motions, *J. Eng. Mech., ASCE* **130,** 1032–1044.

Makris, N., and S. Chang (2000).Effect of viscous, viscoplastic and friction damping on the response of seismic isolated structures, *Earthq. Eng. Struct. Dynam.* **29,** 85–107.

Makris, N., and C. Psychogios (2006). Dimensional response analysis of yielding structures with first-mode dominated response, *Earthq. Eng. Struct. Dyn.* **35,** 1203–1224.

Mallat, S. G. (1999). *A Wavelet Tour of Signal Processing*. Academic Press, New York.

Mavroeidis, G. P., and A. S. Papageorgiou (2003). A mathematical representation of near-fault ground motions, *Bull. Seismol. Soc. Am.* **93,** 1099–1131.

Mavroeidis, G. P., G. Dong, and A. S. Papageorgiou (2004). Near-fault ground motions, and the response of elastic and inelastic single-degree-of-freedom (SDOF) systems, *Earthq. Eng. Struct. Dynam.* **33,** 1023–1049.

Menun, C., and Q. Fu (2002). An analytical model for near-fault ground motions and the response of SDOF systems, in *Proc. Seventh U.S. Natl. Conf. Earthq. Eng.*, Boston, Massachusetts, 10 pp.

Naeim, F. (1995). On seismic design implications of the 1994 Northridge Earthquake records, *Earthquake Spectra* **11,** 91–109.

Newmark, N. M. (1965). Effects of earthquakes on dams and embankments, *Geotechnique*, **15,** 139–160.

Rathje, E. M., N. A. Abrahamson, and J. D. Bray (1998). Simplified frequency content estimates of earthquake ground motions, *J. Geotech. Geoenviron. Eng.* **124,** 150–159.

Ricker, N. (1943). Further developments in the wavelet theory of seismogram structure, *Bull. Seismol. Soc. Am.* **33,** 197–228.

Ricker, N. (1944). Wavelet functions and their polynomials, *Geophysics* **9,** 314–323.

Ruiz-Garcia, J., and E. Miranda (2003). Inelastic displacement ratios for evaluation of existing structures, *Earthq. Eng. Struct. Dynam.* **32,** No. 8, 1237–1258.

Sekiguchi, H., and T. Iwata (2002). Rupture process of the 1999 Kocaeli, Turkey, earthquake estimated from strong-motion waveforms, *Bull.Seismol. Soc. Am.* **92,** 300–311.

Somerville, P., and R. Graves (1993). Conditions that give rise to unusually large long period ground motions, *Struct. Design Tall Buildings* **2,** 211–232.

Spence, R. J. S., A. W. Coburn, A. Pomonis, and S. Sakai (1992). Correlation of ground motion with building damage: The definition of a new damage-based seismic intensity scale, *Proc. Tenth World Conf. Earthq. Eng.*, Madrid, Spain.

Veletsos, A. S., N. M. Newmark, and C. V. Chelepati (1965). Deformation spectra for elastic and elastoplastic systems subjected to ground shock and earthquake motions, *Proc. Third World Conf. Earthq. Eng.*, Wellington, New Zealand, II, 663–682.

Wang, W.-H., S.-H. Chang, and C.-H. Chen (2001). Fault slip inverted from surface displacements during the 1999 Chi-Chi, Taiwan, earthquake, *Bull. Seismol. Soc. Am.* **91,** 1167–1181.

Appendix A

Let us assume that the shape of a mother wavelet $\psi(t)$ supported on a time interval (a, b) satisfactorily matches the predominant pulse of the ground motion, $\ddot{u}_g(t)$. According to equation (12), the values $s = S$ and $\xi = \Xi$, for which the transform $C(s, \xi) = C(S, \Xi)$ obtains its maximum absolute value, offer the scale of the wavelet $w(s)\psi(\frac{t-\xi}{s})$ that locally best matches the signal $\ddot{u}_g(t)$ (in Baker's work, the signal is the velocity time history $\dot{u}_g(t)$). Accordingly, in the neighborhood of the predominant pulse that we are interested in matching,

$$\ddot{u}_g(t) \simeq \lambda(S,\Xi)\cdot w(S)\cdot\psi\left(\frac{t-\Xi}{S}\right) = \lambda(S,\Xi)\cdot\psi_{S,\Xi}(t), \tag{A1}$$

where $\lambda(S,\Xi)$ is a real number. Due to the change of variables, $t \to (t-\Xi)/s$, the support time interval of the wavelet appearing in equation (A1) is $(aS+\Xi, bS+\Xi)$. We now investigate the product of the maximum absolute value of the transform, $C(S,\Xi)$, with the best-matching wavelet, $\psi_{S,\Xi}(t) = w(S)\psi(\frac{t-\Xi}{S})$,

$$C(S,\Xi)\cdot\psi_{S,\Xi}(t) = \left[w(S)\int_{aS+\Xi}^{bs+\Xi}\ddot{u}_g(t)\psi\left(\frac{t-\Xi}{S}\right)dt\right] \times w(S)\psi\left(\frac{t-\Xi}{S}\right); \tag{A2}$$

$$C(S,\Xi)\cdot\psi_{S,\Xi}(t) = w^2(S)\psi\left(\frac{t-\Xi}{S}\right) \int_{aS+\Xi}^{bs+\Xi}\ddot{u}_g(t)\psi\left(\frac{t-\Xi}{S}\right)dt. \tag{A3}$$

Given that we are interested in the neighborhood of the predominant energetic pulse, substitution of equation (A1) into equation (A3) gives

$$C(S,\Xi)\cdot\psi_{S,\Xi}(t) \simeq \lambda(S,\Xi)\cdot w^3(S)\cdot\psi\left(\frac{t-\Xi}{S}\right)\int_{aS+\Xi}^{bs+\Xi}\psi^2\left(\frac{t-\Xi}{S}\right)dt. \tag{A4}$$

The integral appearing in equation (A4) is evaluated with the change of variables $u = (t-\Xi)/S$; therefore, $dt = Sdu$. Accordingly,

$$\int_{aS+\Xi}^{bs+\Xi}\psi^2\left(\frac{t-\Xi}{S}\right)dt = S\int_a^b\psi^2(u)du = SE, \tag{A5}$$

where E is the energy of the mother wavelet. Substitution of the results of equations (A5) and (A1) into equation (A4) gives

$$C(S,\Xi)\cdot\psi_{S,\Xi}(t) \simeq w^2(S)\ddot{u}_g(t)SE. \tag{A6}$$

Accordingly, in the neighborhood of the predominant pulse,

$$\ddot{u}_g(t) \simeq \frac{C(S,\Xi)}{w^2(S)\cdot S\cdot E}\psi_{S,\Xi}(t). \tag{A7}$$

After equating the right-hand side of equations (A1) and (A7), one obtains

$$\lambda(s,\Xi) = \frac{C(S,\Xi)}{w^2(s)SE}. \tag{A8}$$

The multiplication coefficient, $\lambda(S,\Xi)$, given by equation (A8) dictates how much the best-matching wavelet, $w(s)\psi_{S,\Xi}(t)$, needs to be amplified to best approximate the energetic acceleration pulse. In the special case considered by Baker (2007), $w(s) = 1/\sqrt{s}$ and $E = 1$; therefore, $w^2(S)\cdot S\cdot E = 1$, and the multiplication coefficient in equation (A8) reduces to $\lambda(S,\Xi) = C(S,\Xi)$, which is merely the peak value of the wavelet transform, given by equation (12).

Department of Civil Engineering
Division of Structures
University of Patras
GR-26500, GREECE
nmakris@upatras.gr

Manuscript received 20 December 2009